Evaluating the influence of cyclical versus non-cyclical fluvial sedimentation on geothermal flow

Master thesis in Applied Earth Sciences
Faculty of Civil Engineering & Geosciences
Delft University of Technology

Jelmer Doff
Student ID: 4057317
04/04/2021

Author
Jelmer Doff

Title
Evaluating the influence of cyclical versus non-cyclical fluvial sedimentation on geothermal flow.

Advisor
Hemmo Abels

Committee
- Denis Voskov – Petroleum Engineering – GSE Department
- Joep E.A. Storms – Applied Geology – GSE department
- Hemmo A. Abels – Applied Geology – GSE Department

Abstract

To produce accurate 3D fluvial architecture models, it is important to understand the influence of internally generated autogenic controls versus externally generated allogenic controls. When studying a fluvial system, autogenic controls such as river meandering and avulsions generally dominate over 10^3-10^4 years. Allogenic controls such as climate change and tectonics dominate more at time scales of 10^5-10^6 years. A dominant control is astronomical climate change that may produce cyclical fluvial sedimentary successions. The resulting alluvial architecture of autogenic and of allogenic forcing is highly different and it is expected to largely influence geothermal flow through fluvial reservoirs.

The aim of this research is to depict the impact of allogenic (cyclical) versus autogenic (non-cyclical) fluvial sedimentation on geothermal flow. Process-imitating and stochastic based modelling software Flumy is used to generate fluvial facies models where either hypothetical cyclical forcing or hypothetical non-cyclical forcing was the dominant force. These models are subsequently tested for geothermal flow using DARTS (Delft Advanced Terra Simulator).

We find that the Flumy numerical model can be used to produce hypothetical cyclical and hypothetical non-cyclical alluvial architecture. The main difference between the architectures is the shape of the sand bodies. The cyclical model has overall thicker, laterally wider sand bodies. The non-cyclical model has thinner, less wide, but more often connecting sand bodies.

Geothermal flow modelling shows that matching N/G in the cyclical and non-cyclical model in the 20-40 % N/G range gives similar pressures at a constant, fixed water rate. This points to the hypothesis that, at comparable N/G, the well connectivity must also be similar. The non-cyclical model breakthrough times in the 20-30 % N/G range are generally equal or slower, compared to the cyclical model. This gives credence to the hypothesis that the cyclical model has overall equal or slower flow paths between the well connections in the geothermal doublet. The difference in flow path hypothesis can be properly tested through visualizing 3D streamlines and is a recommendation for the future.

Acknowledgements

I would like to thank the many people who helped me during my thesis. First of all, my thesis supervisor Hemmo Abels. He gave me motivation by always being kind and helpful even through video meetings. He often gave me encouragement to finish this thesis.

Denis Voskov especially helped me during the last months and offering advice and useful ideas to continue doing the last part of my thesis, which involved geothermal flow modelling. Without him and his PhD-student Kiarash Mansour I would not have the geothermal modelling results and understanding I do now.

Other members of the TU Delft I would like to thank who helped me over the years with my thesis are my last committee member Joep Storms and in an earlier phase PhD-student Stephan de Hoop. Friends such as Sannidi Shetty and Ahmad Tahir also helped me in some key areas.

And of course, I am grateful to my family and friends giving me encouragement and support. That includes friends I got to know through my jaarclub, rowing and bouldering. Without them I would not have made it. Special thanks to Jade who helped me a lot too over the last year.

Jelmer Doff
Delft, May 2021

Table of Figures

List of Tables

Table of Contents

1. Introduction

Subsurface characterization is done through understanding the structure and conditions of the subsurface. This characterization can be made through the process of predicting the flow of fluids through porous media in a 3D geological model. In other words, this process is commonly called reservoir simulation. This is useful in studies to predict what the effect is of depositional heterogeneity through a fluvial reservoir (Willis et al, 2010).

To perform this 3D subsurface characterization, it is very important to understand and interpret the influence of autogenic and allogenic controls on fluvial systems. These controls critically shape alluvial architecture and thus dominate subsurface fluvial heterogeneity (Abels et al, 2013). Alluvial architecture can be described as the geometry, proportion and spatial distribution of fluvial deposits in the alluvial succession. Gaining knowledge of the alluvial architecture leads to insight into the evolution of fluvial systems (Gouw, 2007).

Landscapes are formed and evolved by intrabasinal processes. These processes are often internally generated in a geological basin and are called autogenic controls. Autogenic controls have the most influence over 10^3-10^4 years and include processes such as river meandering and channel avulsion. External (allogenic) controls such as climate change, tectonics and eustacy are more steady over these smaller time scales and are best perceived at time-scale intervals of 10^5-10^6 years (Hajek et al, 2012) (Stouthamer et al, 2007). An important factor is river avulsion, which is the process of shifting part or all of the channel belt to another location on the floodplain. River avulsion frequency determines the spacing of channel belts in alluvial stratigraphy (Stouthamer et al, 2011).

Avulsion is controlled by both autogenic and allogenic processes, but their relative roles are not well known. Examples of how avulsions are controlled by these processes include the changing of the stream power, cohesion of banks and superelevation of the channel or the channel belt above the floodplain (Stouthamer et al, 2007). To show the interaction between autogenic and allogenic processes a surface with mountains can be considered, going through alluvial plains, and extending into a marine environment. This is portrayed in Figure 1.1. The red boxes represent external controls, the blue boxes are internal autogenic controls, while the grey boxes are stratigraphic patterns as a result of both controls (Hajek et al, 2017). Abels et al, 2013 found local avulsions, at least in the Bighorn Basin, to be autogenic in nature. Conversely, they hypothesized that times of extreme floods caused regional avulsion. The intervals in between these regional avulsion cycles are then more stable. These intervals were found to be at astronomical precession climate cycles (Abels et al, 2013).

In a fluvial environment, allogenic controls leave changes in upstream and downstream conditions. These changes can be water discharge and sediment supply variations driven by the climate, subsidence and exhumation driven by tectonics and base level fluctuation driven by tectonics and/or the climate. The changes in conditions may be cyclical when they are related to the orbital cycles, which were important in climate changes previously. That's why climate cycles that are astronomically driven could cause cyclicity in alluvial depositional records (Wang et al, 2021).

Autogenic processes could destroy astronomically-driven climate cycles conditions before they have a chance to be preserved in stratigraphy. As such the cyclical (allogenic) conditions may not be present in stratigraphic records in systems which have large autogenic dynamics. In a fully autogenic modelling scenario compensational stacking occurs, while this is interrupted in a model with allogenic forcing present. Also the stochastics involved in channel bifurcation and avulsion give unpredictable behaviour in models which could be to a great extent close to how autogenic processes work in reality (Hajek et al, 2017).
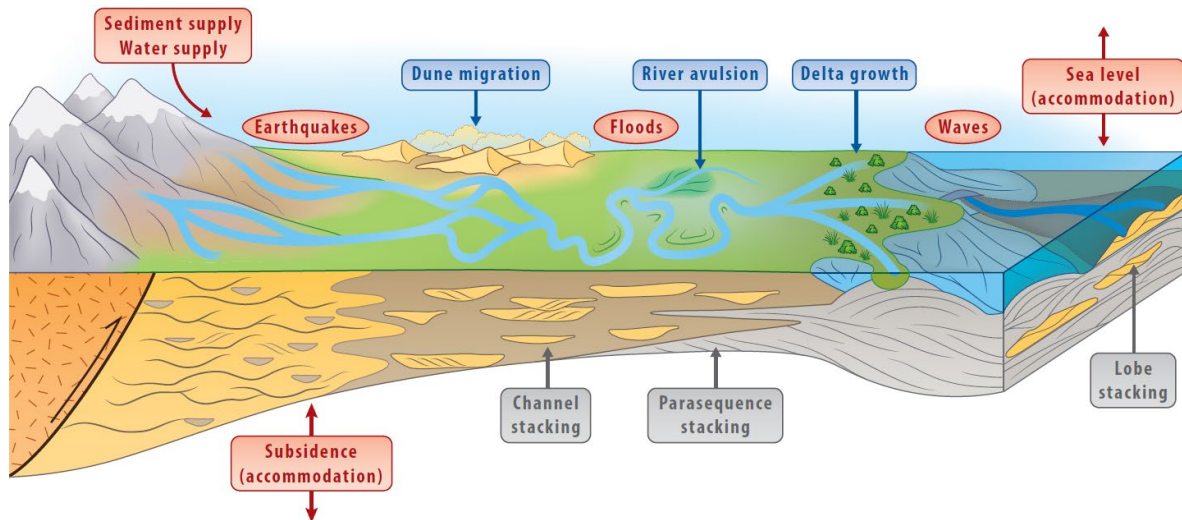
Figure 1.1: Showing the interaction between the allogenic and autogenic processes. Consider a surface with mountains, going through alluvial plains, and extending into a marine environment. The red boxes represent external controls and the blue boxes are internal controls, while the grey boxes (stacking of deposits) are stratigraphic patterns as a result of both controls (Hajek et al, 2017).

1.1 Geothermal energy

In this thesis the application of the models is focussed on geothermal energy. Geothermal energy can be described as the energy contained as heat in the subsurface. The heat comes from the physical processes occurring in the internal structure of the Earth and is present in huge, almost inexhaustible quantities. Despite this, it is unevenly distributed and often not concentrated. Most of the time the heat is also too deep for viable exploitation. An example of an area with viable geothermal exploitation is near magma bodies (Barbier, 2002).

To extract and utilise the heat a carrier is needed to guide the heat toward accessible subsurface depths. There are two forms of heat transfer within the earth, which are conduction and convection. Conduction is the transfer of random kinetic energy without material physically moving. It is the primary cause of heat transfer in solids. Metals are good conductors, while most rocks are bad conductors. Convection is the usual heat transfer mode in liquids and gasses. It is the movement of hot fluid to another place and since physical movement occurs it is a much more efficient process compared to conduction. The high temperature and pressure aquifer reservoirs occurring through convection are essential in most geothermal fields (Barbier, 2002).

There are four main requirements needed to make a geothermal resource viable for exploitation. A heat source such as a magma body is needed. It also needs a carrier of heat such as a fluid and a permeable fluid pathway for production. The last requirement is a cap rock to confine the convection fluid in the reservoir (Okandan, 2012).

Based on the temperature ranges, the geothermal systems are classified as follows. The first are low enthalpy systems which occur below 120˚C or 393.15 K. There are also high temperature systems occurring above 120˚C or 393.15 K. Lastly there are hot dry rock systems requiring external circulation and production of heated fluid). Low enthalpy systems are best for direct heating application as the fluid exists as a liquid in the reservoir. In contrast to that high enthalpy systems can be used for electricity production. In these systems the substances could all be liquid, gas or both (Okandan, 2012).

A geothermal reservoir can be exploited through the use of well doublets. A doublet is a pair of wells with one well acting as an injector and the other as a producer. The producer well produces the hot fluid from the reservoir used for e.g. heating and through the injector well the colder fluid (after its application) is injected again. This provides pressure in the reservoir needed to keep producing the hot fluid (Wachowicz-Pyzik et al, 2020).

1.2 Modelling tools

A static facies modelling tool, both process-imitating and stochastic, called Flumy is utilized in this thesis. This means that Flumy imitates the physical processes used to simulate a river, while the stochastic element provides different realizations of every simulation run. Previous research was done using Flumy on a connectivity analysis, but not yet in relation to allogenic forcing. It was discovered that there were several main factors that determine the chance sandstone bodies connect in sedimentary reservoirs. These were the net-sandstone volume (N/G), the sandstone body geometry and the range in paleo-flow direction. It is recognized that in meandering fluvial reservoirs, the N/G threshold for under which isolated sand bodies occur is often between 20% and 30% N/G. This also depends on the sand body geometries (Willems et al, 2017). Facies modelling affects both the spatial distributions and the shape of the sand bodies, and thereby also the connectivity (Villamizar et al, 2015).

The Delft Advanced Research Terra Simulator (DARTS) is used in this thesis for geothermal flow modelling. It is proven to provide fast and accurate energy production evaluation for geothermal exploitation. It is demonstrated that DARTS provides good results for both low enthalpy and high enthalpy systems in comparison with other geothermal simulators like TOUGH2 and ADGPRS. It also allows for high performance and a flexible code which makes it useful for the quantification of uncertainty. A sensitivity analysis has been done for several different production regimes and geological properties in realistic geothermal case studies. This sensitivity analysis entailed well management as well as different permeability ratios, permeability-porosity correlations and fault connectivity (Wang et al, 2019).

1.3 Research goal and hypothesis

The aim of this study is to evaluate the impact of allogenic (cyclical) versus autogenic (non-cyclical) fluvial sedimentation on geothermal flow. The following research questions help to answer the evaluation of the study:

- Can hypothetical cyclical and non-cyclical alluvial stratigraphy be produced using Flumy modelling?
- What is the impact of the different alluvial stratigraphies of the cyclical and non-cyclical models on geothermal flow?

Autogenic behaviour is sometimes ordered or patterned, this is referred to as self-organisation in Hajek et al, 2017. An example of this is a regular spacing of point-bars in meandering rivers. Orbitally-forced allogenic behaviour is always ordered and causes cyclic deposition (Abels et al, 2013). This means that sediments in that environment are always deposited over a set period of time. Both allogenic and autogenic behaviour being ordered could be an indication that there is a comparable amount of connectivity in both.

Autogenic and allogenic controls affect sand body thicknesses and thickness of shale layers in between the sand bodies. These are factors that influence the lifetime and doublet performance of a geothermal reservoir and as such should influence the created cyclical and non-cyclical models (Crooijmans et al,

2016). Other human made factors such as the well spacing in a geothermal doublet affect the life time of a fluvial reservoir significantly (Willems et al, 2017).

Reservoir connectivity can be defined as the ratio of the volume of the largest connected reservoir body over the sum of the volume of all reservoir bodies. This connectivity is firmly linked with the N/G in the reservoir. Between 10-20 % N/G the connectivity is the most sensitive in fluvial systems (Crooijmans et al, 2016).

1.4 Thesis approach and structure

The workflow was as follows. A modelling tool, both process-imitating and stochastic, called Flumy was used to create different static facies models. Flumy can model a meandering channel and its associated deposits, such as point-bar sands, and overbank flow deposits. It can show the evolution in time of the channel by migration, cut-off and avulsion (Flumy manual, 2017). This makes it suitable for the research since cyclical and non-cyclical forcing happen over different time scales. Chapter 2 starts with a brief background on Flumy modelling after which a sensitivity analysis on Flumy is given. Furthermore this chapter explains the step-by-step methodology on how the static hypothetical cyclical and non-cyclical facies models were acquired. The cyclical model was created using data value influences from the Bighorn Basin area, but is not considered to be based on it since that could not be accurately done. The cyclical and non-cyclical models are hypothetical, since they are different from those created in previous work by Abels et al, 2013 and Wang et al, 2021. The main difference is that only regional and local avulsion is varied in the static models created through this study. Then, chapter 3 starts with an introduction to DARTS geothermal modelling. After testing and evaluation one hypothetical cyclical and one hypothetical non-cyclical model were chosen for assessment and a comparison is done through dynamic geothermal flow modelling. Chapter 4 includes the discussion on the results and chapter 5 presents the conclusions drawn and further research recommendations.

2. Flumy Modelling

This chapter presents a brief background of Flumy in subsection 2.1 after which a sensitivity analysis of Flumy is given in subsection 2.2. Subsection 2.3 describes the workflow from which the static hypothetical model results are produced. The model results are then presented in subsection 2.4.

2.1 Modelling background

In this subsection some concepts are explained relating to the modelling simulations. These concepts are useful for the interpretation of the simulation results. Avulsion and aggradation in modelling are described. The general concept of Flumy is reported and several important parameters used in Flumy are explained.

2.1.1 Avulsion and aggradation

In the Flumy model there is a distinction between regional and local avulsions. Regional avulsion can be considered to be caused by successful levee breaches upstream and occurs upstream in the domain. This results in an entirely new path within the domain. The domain in Flumy is later explained in Figure 2.3. The regional avulsion period is expected to be longer than the period for local avulsions. Lower avulsion frequency means a more meandering channel, and thus more complex systems and a wider sand body deposition, also known as the channel belt. Local avulsion happens through a bifurcation within the domain (Flumy manual, 2017).

Stouthammer et al, 2007 suggests that a way to improve modelling of avulsions (and thereby fluvial architecture) is to know which autogenic and allogenic factors influence avulsion. And that it is also useful to know the relative importance of these factors in time and space.

Another important concept is aggradation. In reality, river avulsion is, among others, regarded to be driven by aggradation (Törnqvist et al, 2002). Spatial patterns of overbank aggradation rate over stratigraphically relevant time scales are vital models of fluvial system in avulsion dominated models. Regarding the Flumy facies model, there are several important model parameters related to aggradation, such as overbank flow occurrence and thickness, and the thickness exponential decrease of the floodplain. These are described more extensively in the next section.

2.1.2 Flumy modelling software

A goal of this thesis is to create a hypothetical cyclical and non-cyclical static facies model after which it is then used for dynamic flow simulations. Designed by MINES ParisTech, fluvial architecture modelling software Flumy can accomplish this (Lopez et al, 2001, 2008). Flumy version 5.5 was used and is both a process-imitating and stochastic modelling software. It uses a working space in which the domain is discretized as a rectangular 2D grid. It creates a meandering channel with a channel belt and flood plains. The channel can flow in both the x and y direction. In Flumy "time" is discretized into iterations. In these time steps migration is performed. 1 iteration can be thought of as 1 year in time. (Flumy manual, 2017)

Flumy's model construction can be considered in three main processes: Channel migration which deposits point bar sand bodies, aggradation caused by overbank floods, and channel wandering due to avulsions which can possibly lead to the creation of new channel paths. These processes are shown in Figure 2.2 along with all the possible model deposits (Bubnova A, 2018).
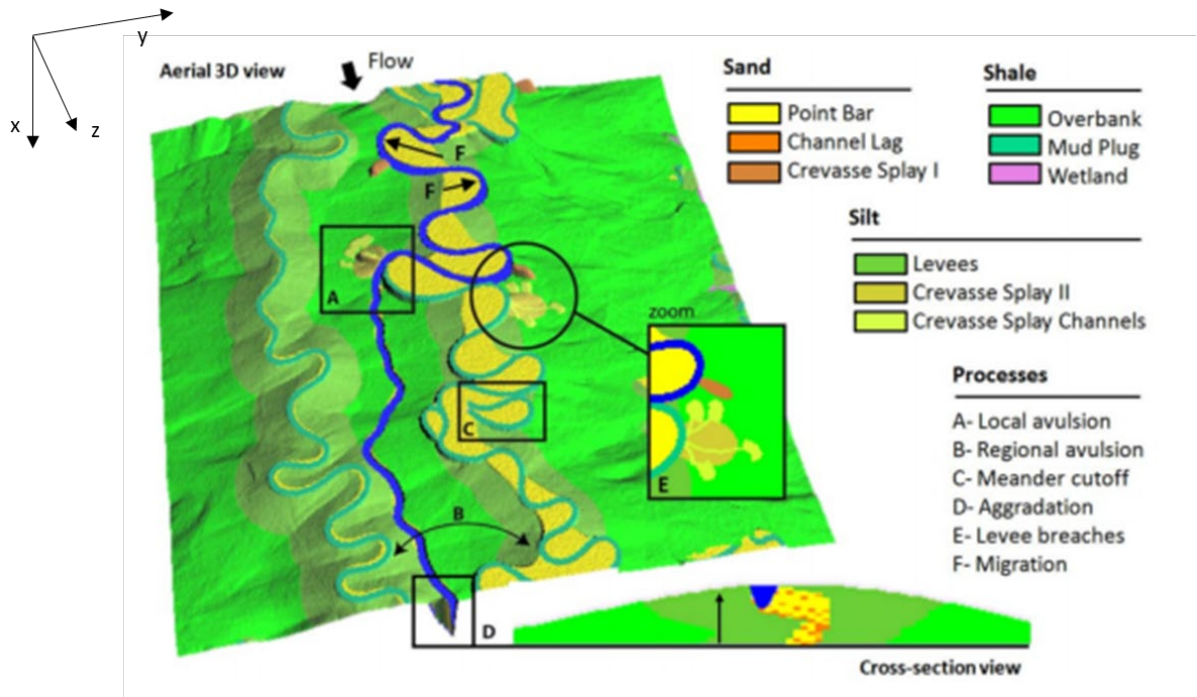
Figure 2.1: Showing the Flumy processes, top view and cross-section view. Also the various deposits are displayed (Modified from Bubnova, 2018).

2.1.3 Flumy parameter explanation

There are many parameters which can be used and tweaked in Flumy, but the most relevant parameters for the research purpose are listed as follows in Table 2.1. The hypothetical cyclical model was influenced by data values from the Bighorn Basin in Wyoming (USA) since in that area evidence was determined of allogenic controls, specifically due to climate change (Abels et al, 2013). However, In this thesis the cyclical model is only considered to be inspired from it, not based on it, since that could not be accurately done.

Parameter	Process
Model dimension and paleoflow direction	Migration
Channel depth, channel depth and channel wavelength	
Regional and local avulsion frequency (periodic).	Avulsion
Overbank flow occurrence	Aggradation
Overbank flow deposit maximum thickness	
Overbank flow deposit exponential decrease	

Table 2.1: The relevant Flumy parameters for the research purpose and the associated process influenced by these parameters.

By varying the migration, avulsion and aggradation processes contrasted architectures can be simulated. Since it is a stochastic model, different realizations of the model can be generated using the same input parameters values. The only difference is these simulations will have different seeds. Later on this aspect is used to test the variation in the cyclical and non-cyclical models (Bubnova, 2018).

- **Model Dimension and Paleo flow direction**
  The model domain of the channel basin considered in this report has the dimension of 30000m x 15000m x 100m, which are respectively the length, width and height of the model (Table 2.2). The standard model has a grid lag size of 50m x 50m x 1m. These grid lags are chosen since Flumy requires a certain ratio between parameters. For example, if the channel width has a specific size, the size of the grid lags needs to be small enough otherwise the model

resolution doesn't capture it as accurately as it could be. The grid lags also need to be as big as possible to reduce the simulation time. The influence of these relations is later discussed in a sensitivity analysis.

These model dimensions mean that the number of grid cells in each direction is 600 x 300 x 100. This means that the 100m of thickness that Flumy generates is vertically averaged to 1 m for each layer. Thus essentially there are 100 layers of 1 m in the z-direction. The paleocurrent flow direction was set along the longest side of the model which in our case is along the x-direction. All this is summarised in Table 2.2 below.

Parameter	Value
Model dimensions (L x W x H) (m)	30000 x 15000 x 100
Number of grids	600 x 300 x 100
Size of each grid cell (grid lag) (m)	50 x 50 x 1

Table 2.2: Model dimension parameters used in the chosen standard model.

- **Channel depth, channel width and channel wavelength.**
  The channel depth, channel width and channel wavelength were set respectively to 4m, 60m and 750m. These variables could accurately represent a channel in a basin of this size. The channel width and depth are generally a bit smaller in the Bighorn Basin, but are still similar (Foreman et al, 2012).

- **The avulsion frequency**
  Flumy allows the user to control the frequency of both types of avulsions: regional and local avulsions. To simulate the cyclic and non-cyclic models both the regional and local avulsion was periodically set and varied, with sometimes an infinite period. This is better explained in chapter 3.1, the static model methodology.

- **Overbank flow occurrence**
  Overbank flow floods the surfaces of the floodplains. Data from the Bighorn basin doesn't tell us anything about any flooding occurrence as well as the following two aggradation parameters. One option was to look at previous work done with Flumy, although those were done with smaller domains (Crooijmans et al, 2016) (Hamm & Lopez, 2012) (Willems et al, 2017). Another option was then to adjust the input for the bigger domain such as the one in the Bighorn Basin. This includes similar sand body sizes and amount of deposition relative to the time passed. Eventually, to match the desired simulation outcome, the value of this parameter for the cyclical and non-cyclical model was set to every 300 iterations/years.
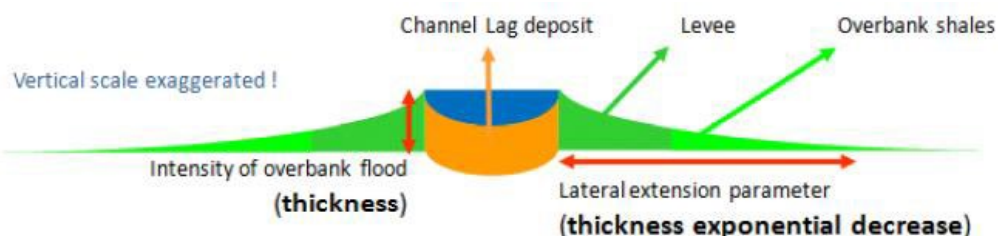
Figure 2.2: Image sourced from Flumy manual to demonstrate thickness exponential decrease and maximum thickness of over bank flow deposits.

- **Overbank flow deposit maximum thickness**
  As can be seen in Figure 2.2, this parameter determines the thickness of overbank flow deposits. A lower value of this parameter means fewer clay sediments deposited on the floodplain. This means there is relatively more sand and increases the N/G of the model. This parameter was set to a value of 0.2 m for the cyclical model, but was changed for the non-cyclical model.

- **Overbank flow deposit thickness exponential decrease:**
  Regarding Figure 2.2 again, this parameter determines the scaling distance of the negative exponential distribution which rules the decreasing of deposits thickness away from the channel. When this is set to a higher value, it increases the width and thickness of floodplain deposits. Consequently, this also increases the aggradation rate. After some consideration to get the desired outcome explained before, this parameter was set to a value of 6000 m.

All other possible input parameters such as the erodibility coefficient and the global slope along the flow direction were set to standard values. This was done since these parameters were researched and afterwards were decided to be less important and judged to be fine for the facies model output purpose of this thesis. It is important to consider that while Flumy's deposits sediment inside the domain, it also (invisibly) deposits sediment outside the domain in the domain margin. This is illustrated in Figure 2.3. The reason for this is to remove border effects within the domain when the channel is migrating or aggradating. The default value for the domain margin equals 12 times the channel width and also corresponds to the development of at least one meander.
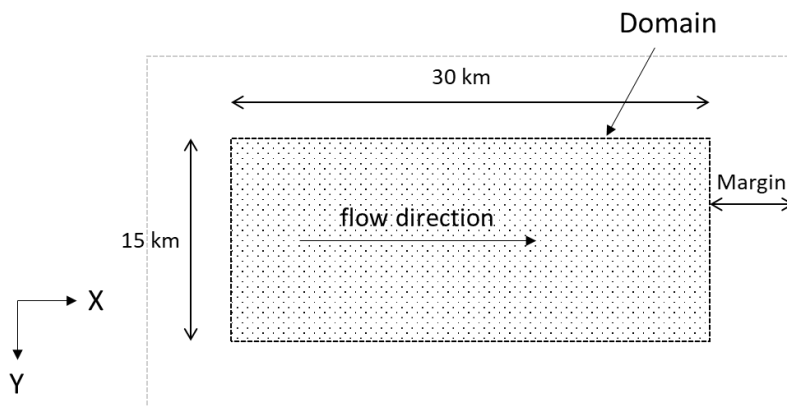
Figure 2.3: Explanation of the Flumy domain and it's domain margins. Flumy deposits sediment inside the domain as well as (invisibly outside the domain in the domain margin.

2.2 Sensitivity analysis

The sensitivity analysis is divided up in three parts. First the Flumy input parameters are tested for their sensitivity, after which it is decided which parameter values are best suited for this research purpose. Concluding, a few comments on the sensitivity of the DARTS flow model using our specific facies model are given.

First of all, it should be mentioned some sensitivity analysis between some parameters was already done in subsection 6.3 of the Flumy user manual, although this was brief and not quantitative. Here a more quantitative approach is implemented to test how parameters are influenced using a model with a large domain and large avulsion periods. It should also be mentioned that the Flumy manual contains a "usual range of values" table in subsection 6.2. This mentions the range of values that are realistic, such as that the ratio between channel width and depth should not exceed a certain number. It also gives relationships, such as that model channel width should be a certain size bigger than the channel width, otherwise the meander loops will not be sufficiently simulated. These usual ranges of values and relationships are all adhered to, although it is discussed later when this is not the case. Specifically, the aspect related to some parameters and the resolution are later discussed.

Now, the sensitivity analysis was performed using parameter ranges mentioned in Table 2.1. The ranges were determined using the help of the "usual range of values" subsection 6.2 of the Flumy user manual, although not all parameters in Table 2.1 are mentioned there. The question that was answered is for what value or range the parameters used was best suited to the research purpose. These suited input parameters are later shown in Tables 2.3 and 2.4. When testing the different parameters, only the parameter that was tested was changed. In Table 2.1 some general effects are mentioned of the input parameters on the output parameters shown in Table 2.2.

Input parameter	Input parameter range	Influence on output parameters
Domain:		
Horizontal grid lag (cell size in X & Y – direction; Horizontal resolution)	10 – 100 m	No notable effect, except lower resolution means lower modelling time relative to amount of deposition.
Horizontal grid size (length x width, taken as the same value)	1 – 40 km	Higher grid size means all output parameters are relatively lower, while modelling time goes up.
Channel parameters:		
Maximum depth	2 – 6 m	Channel parameters are more difficult to quantify since they have to be (fairly close to) multiples of each other to be realistic.
Width	20 – 60 m	Channel width has similar effects as channel depth, this means higher input creates higher N/G, less aggradation, not much effect on mean topography/floodplain slope/modelling time.
Wavelength	125 – 750 m	The difference with the other parameters are that a higher wavelength creates less N/G, negligible effect on aggradation and more mean topography.
Avulsion parameters:		
Regional avulsion (periodical)	2000 – 30000 iterations / years	With a longer period, both avulsion parameters have a negative effect on N/G, not much effect on aggradation, and a positive effect on mean topography, floodplain slope and modelling time.
Local avulsion (periodical)	500 – 8000 iterations / years	Difference in intensity of effects on output parameters, regional avulsion has a bigger overall effect.
Aggradation parameters:		
Overbank flooding occurrence (periodical)	50 – 600 iterations / years	A higher flooding occurrence creates less floodplain.
Floodplain sediment maximum thickness	0.01 – 0.6 m	Opposite to the occurrence, a higher floodplain sediment max. thickness creates more floodplain.
Floodplain sediment thickness exponential decrease	500 - 8000	This creates above all a much more stretched out floodplain, so has a big effect on mean topography.

Table 2.3: Parameter ranges used in the sensitivity analysis. The ranges were determined by taking into account the "usual range of values" from subsection 5.2 of the Flumy user manual, and seeing what effect they have on the model.

The "input" parameters mentioned in Table 2.1 are compared to the chosen "output" parameters, which are the Net to Gross, the aggradation rate, the mean topography, the Floodplain slope, and the modelling time vs amount of sediment deposition.

Most parameters behaved logically with an expected outcome. Still, sometimes unexpected outcomes happen which can sometimes not be explained. This appears to be just an error or a bug in Flumy.

Most often when using the same parameter values the expected outcome happens. It is important to remember that Flumy creates facies models stochastically, which creates variance as well. Still, there is a certain type of continuity in the output presented parameters. To keep it fairly simple, clear and understandable, only these signs are used in Table 2.2 and are as follows: "-", "+", and "=". When there is no correlation (or almost no noticeable) it is mentioned as "=", "-" when an increase in the input parameter creates a decrease in the output parameter, and "+" when an increase in the input parameter creates an increase in the output parameter. When the relation between the input and output parameter creates no, or a negligible relationship, it should be noted that this may be because of the ranges chosen in Table 2.1. However, these range cannot be changed much, since otherwise not a realistic model is simulated.

Output: Input:	Net to Gross (N/G)	Aggradation rate	Mean topography	Floodplain slope (gentler [<] or steeper [>])	Modelling time relative to amount of deposition (faster [<] or slower [>])
Domain:					
Horizontal resolution	=	=	=	=	+
Horizontal grid size	-	-	-	-	+
Channel *dimension* parameters:					
Max depth (m)	+	-	=	=	=
Width	+	-	=	=	=
Wavelength	-	=	+	=	=
Avulsion parameters:					
Regional avulsion period	-	=	+	+	+
Local avulsion period	-	=	+	+	+
Aggradation parameters:					
Flooding occurrence (higher or lower period)	+	-	-	-	+
Floodplain sediment maximum thickness	-	+	+	+	–
Floodplain sediment thickness exponential decrease	-	+	+	-	-

Table 2.4: Results of the sensitivity analysis between the input parameters on the left side of the table and the output parameters chosen on the right side of the table. The meaning of the signs in the table are as follows: "=" when there is no correlation (or almost no noticeable for the chosen input parameter range), "-" when an increase in the input parameter creates a decrease in the output parameter, and "+" when an increase in the input parameter creates an increase in the output parameter.

Following the results in Table 2.2 and the comments in Table 2.1, it is useful to offer further explanations.

Looking at the domain, the horizontal resolution (to a certain degree) does not have a noticeable effect on any of the output parameters, except for the modelling time relative to the amount of sediment deposition. It makes sense that for a higher resolution, much more calculations need to be made. This makes it takes a longer time for the same amount of deposition. It also makes sense that a higher grid size makes for a lower overall N/G, aggradation rate, mean topography (total amount of deposition) and floodplain slope.

The channel dimension parameters are a bit harder to quantify. This is because all of them are related to each other in the sense that for them to be realistic they have to be (close to) multiples of each other. The channel width has to be about fifteen times the channel maximum depth, while the channel wavelength has to be about 12.5 times the channel width (Flumy manual, 2017). These relations make them not realistic any more when one parameter is too far off. Still, some parameter sensitivity can be derived when the parameter is not taken to extremes.

Now, looking at the channel width and depth there is a similar amount of positive difference in the Net to Gross output when going through the ranges in Table 2.1. In contrast, a bigger channel wavelength creates a lower N/G. The wavelength does not seem to have a big effect on aggradation rate and also influences the mean topography much more than the channel width and depth. In other words, the difference in channel wavelength makes for a bigger difference in how much sediment is deposited in total, relative to the channel width and depth. All of the channel parameters don't seem to have a big effect on the modelling time relative to how much is deposited.

The local and regional avulsion have the same effect on the output parameters, but there is definitely a difference in the intensity of the effect. A higher regional avulsion has a bigger negative effect on the N/G than the local avulsion. The difference in modelling time is also much bigger when varying the regional avulsion. This makes sense since the range of the value tested for the regional avulsion is also much larger. The avulsion parameter fundamentally changes the resulting model much more than most other input parameters.

As expected, the overbank flooding occurrence period and the maximum thickness of the floodplain sediment have opposite reactions. This is logical since a higher flooding occurrence period means less deposition of floodplain, while a higher floodplain sediment thickness means more deposition of the floodplain. The difference between those two input parameters lies in how much total sediment is deposited (mean topography) and in the floodplain slope. The flooding occurrence creates a much bigger difference in mean topography and in the slope of the floodplain.
A higher thickness exponential decrease also makes for a much more stretched out floodplain, so that the floodplain becomes much wider. This creates much more total sediment deposition and a much gentler floodplain slope.

2.3 Methodology to produce the non-cyclical and cyclical static facies models

This section describes the workflow to obtaining the hypothetical cyclical and non-cyclical models for comparison.

Step 1.
First the model parameters used in Flumy were studied to understand how they work and interact with the rest of the model. The Flumy user manual was a big help in this regard, but also some research papers on the Flumy model had to be studied to help with the understanding of the parameters (Bubnova, 2018) (Crooijmans et al, 2016) (Hamm & Lopez, 2012) (Willems et al, 2017). For example, it is important to know which parameter influences the Net to Gross or how to get isolated vs stacked sand bodies. The trial and error method of studying helped to achieve this.

Step 2.
After the parameters and their relations to each other became clear, the important parameters were distinguished from the less important parameters. These are the parameters that have significant impact on matters such as N/G, floodplain deposition and the connectivity of the sand bodies. These specific parameters are discussed in Flumy background subsection 2.2.

Something that should be taken into account is that there are parameter relationships. This means that there are certain ranges, maximum or mean values for some parameters. These relationships are described in subsection 6.2 of the Flumy user manual published in 2017. The relationships were compiled from natural and experimental observations. Outside of these ranges the model would not be realistic.

There were some problems with this which are as follows. With a model domain of a length and width of 30km x 15km, the model would naturally become fairly slow. Something to help with this is to make the individual grid cells (grid lags) as large as possible. Unfortunately, the grid lags also have a restriction related to the channel width. With larger grid lags, the channel width also needed to be larger. This created a problem with the resolution being too coarse to accurately capture the channel. This in turn can cause too much sand deposition in the model. It should be remarked that this effect on the (horizontal) resolution does not seem to be that big up to a certain point. This is further discussed in the sensitivity analysis in subchapter 2.2.

Step 3.
A sensitivity analysis was done to further try to completely understand Flumy. Every proclaimed important input parameter in Flumy was varied to try to find out its influence on a few certain important output parameters. Ranges of these parameters were taken after which it was analysed what ranges (or single values) work best for the purpose of this thesis. Certain output parameters were chosen to do this analysis. The influence of the different input parameters was looked at for the Net to Gross of the 3D block, the aggradation rate, the mean topography (mean amount of sediment deposited), the slope of the floodplain, and the effect on how fast sediment is deposited (amount of years/iterations needed for an amount of sediment deposition).

Step 4.
The aim was to make hypothetical cyclical and non-cyclical static 3D facies models using Flumy. The models are hypothetical since only regional and local avulsion is changed in the models, which is different compared to cyclical models in previous work by Abels et al, 2013 and Wang et al, 2021. To best compare the non-cyclical and cyclical runs, the focus was for both types of runs to have a similar amount of sediment deposited in a similar time frame. This means to fill the 3D blocks in a similar amount of years/iterations. That is why for the relevant parameters fixed standard values are chosen

(as described in subsection 2.1), except for the regional and local avulsion. The parameters were also chosen such that sand bodies were deposited with similar vertical thickness to create a better comparison.

As is discussed, the hypothetical non-cyclical runs use the same parameters as the hypothetical cyclical runs with two notable exceptions as shown in Table 2.3. The overbank flooding maximum sediment thickness was changed to a range of 0.2 to 0.6 m to generally create thicker floodplains. This was to offset the relatively much more often occurring local avulsion (vs regional avulsion) which creates more much more sand deposition. A test of this is presented later in Figure 2.12 and Figure 2.13. Another change in the non-cyclical run was that the local avulsion is varied from a period of 1000 till 6000 iterations to better understand the effect it has on the sand body dimensions, sand body position relative to the clay and the time of deposition. Regional avulsion was set to an infinite period.

Process	Parameter	Value
Migration	Model dimensions (L x W x H) (m)	30000 x 15000 x 100
	Number of grids	600 x 300 x 100
	Size of each grid cell (grid lag) (m)	50 x 50 x 1
	Maximum depth (m)	4
	Width (m)	60
	Wavelength (m)	750
Avulsion:	Regional avulsion (iterations) (periodically)	**Infinite**
	Local avulsion (iterations) (periodically)	**500; 1000; 500; 1000; 2000; 3000; 4000; 5000**
Overbank flooding: (aggradation)	Occurrence (iterations) (periodically)	300
	Maximum sediment thickness (m) (uniform range)	**0.2 – 0.6**
	Thickness exponential decrease.	6000

Table 2.5: Parameters used in the hypothetical non-cyclical runs. The differences with the cyclical runs (boldly projected) are that the maximum sediment thickness from overbank flooding is a uniform range between 0.2 and 0.6. The local avulsion is varied from a period of 1000 till 6000 iterations, while the regional avulsion is set to an infinite period to ignore this parameter.

Moving on to the cyclical runs, one type of optimized run was devised that would follow the hypothesis that in long term climate affected environments sediment is deposited in sequences following the 20000-year precession Milankovitch cycle (Abels et al, 2013). That is why the in the cyclical runs the regional avulsion value of 20000 years was chosen and the local avulsion parameter was ignored and disabled. The local avulsion was set to an infinite period. The parameters chosen in the cyclical runs are summarised in Table 2.4.

Process	Parameter	Value
Migration	Model dimensions (L x W x H) (m)	30000 x 15000 x 100
	Number of grids	600 x 300 x 100
	Size of each grid cell (grid lag) (m)	50 x 50 x 1
	Maximum depth (m)	4
	Width (m)	60
	Wavelength (m)	750
Avulsion:	Regional avulsion (iterations) (periodically)	**20000**
	Local avulsion (iterations) (periodically)	**Infinite**
	Occurrence (iterations) (periodically)	300
	Maximum sediment thickness (m) (constant)	**0.2**

Overbank flooding: (aggradation)	Thickness exponential decrease.	6000

Table 2.6: Parameters used in the hypothetical cyclical runs. Differences with the non-cyclical are projected in bold. The difference with the non-cyclical runs are that the regional avulsion parameter is set to a period of 20000 years/iterations, while the maximum sediment thickness when overbank flooding occurs is set to a constant 0.2 m.

Step 5.
From these model simulations cross-sections were taken to compare the different kinds of runs. Most often the chosen cross sections were perpendicular to the flow direction, since the best comparisons can be made relative to cross-sections in other positions. Many differences between the runs were compared and contrasted such as, among others, the connectivity inside the models and the net-to-gross.

Step 6.
Concluding, a 3D block was exported from Flumy into Petrel to visualize the facies model in 3D. This helped to further understand the model by sifting through cross sections in the block. This is possible in all 3 directions. (x, y and z) Using this, a better understanding of the connectivity in the model was achieved. Using Petrel and Matlab the N/G was determined.

2.4 Static modelling results

In this subsection the facies model results of the hypothetical non-cyclical simulation runs are presented, after which the hypothetical cyclical simulation runs are shown. After analysis one non-cyclical run and one cyclical run are picked for comparison using geothermal flow simulations in DARTS.

2.4.1 Non-cyclical runs

Several hypothetical non-cyclical runs were performed, with varying amounts of local avulsion periods. This was done to determine which run and corresponding local avulsion period would produce the most similar simulation result as a cyclical run. The results are analysed with the help of representational cross-sections of each run. Each non-cyclical run has exactly the same input parameters as the others, except for 2 differences. They each have a different local avulsion period and are assigned a different seed. The simulation is stochastic and the seed value is used to generate the series of random numbers. Any simulation can be reproduced if the same seed value is taken when taking the exact same parameter values. Contrary to the cyclical runs, which are discussed later, no regional avulsion was simulated. Thus, the regional avulsion period was set to infinite.

The results of all the different runs are summarised in Table 2.5. Looking at the N/G in all the runs a pattern is recognized. When a run has a lower local avulsion period, the resulting N/G will generally be larger since more sand is deposited. This is not always true, since non-cyclical runs in general seem to have quite a bit of variance due to the stochastic simulation in the resulting facies model. As an example *Run 1* with a local avulsion period of 500 years has a lower resulting N/G than the resulting N/G from *Run 2*, with a local avulsion period of 1000. The same happens with *Run 3* vs *Run 4* and *Run 8* vs *Run 7*.

Non-cyclic run #	Local avulsion period (iterations/years) (input)	N/G	Sand body vertical thickness (average)	Sand body vertical thickness (range)
1	500	36,3 %	9m	4m - 17m
2	1000	37,6 %	10m	4m - 25m
3	1500	32,1 %	11m	4m - 22m
4	2000	32,4 %	10m	4m - 23m
5	3000	28,4 %	12m	4m - 32m
6	4000	24,6 %	13m	4m - 28m
7	5000	23,4 %	14m	4m - 34m
8	6000	25,0 %	13m	4m - 33m

Table 2.7: The hypothetical non-cyclic runs and their differences. Only one input parameter was changed for all the runs, this was the local avulsion period. The resulting output parameters are displayed as well. These are the N/G, the sand body vertical thickness (average), the sand body vertical thickness variation (range).

Vertical sand body thickness

There are also differences in vertical sand body thicknesses between the runs. This was measured by taking 25 measurements all over each facies model run, after which an average was calculated to a whole meter in Table 2.5. The runs with lower avulsion periods have less accumulated/stacked sand bodies. This is most evidently seen in the cross-sections of *Run 1* and *Run 2*. This can be observed in respectively Figure 2.4 and Figure 2.5. All the cross-sections are taken in the Z,Y-plane and are perpendicular to the flow direction in all the 3D models. In all the cross-sections the yellow deposits are point bars, grey are sand plugs, green are floodplains, dark green are levees, turquoise are mud plugs, and orange are channel lags. Figure 3.1B clarifies the position of all the cross-sections in the 3D blocks. The cross-sections from all runs are taken at the same position in the 3D block. In *Runs 5 till 8* there is a significant increase in the average sand body vertical thickness. This is visible in Figures 2.7, 2.8, 2.9, 2.10 and also in Table 2.5. The increase in thickness is not very large, with only 5 meters between *Run 1 and run 7*. It makes sense that the minimum sand body thickness is 4m since the channel depth input parameter is also 4m. The maximum sand body thickness also seems to get larger in the runs with a higher local avulsion period.

Connectivity

Looking at the connectivity in the model results there are definitely a few differences between the runs as well. *Run 1* and *Run 2* overall have fairly homogenous good connectivity over the whole model. This is evidenced in the cross sections of Figure 2.4 and 2.5. This becomes noticeably worse in *Run 3* and onwards. This is not a surprise since the N/G also becomes noticeably lower in *Run 3* and onwards. The connectivity is the worst in *Run 8*, where the N/G is similar to *Run 6* and *Run 7*.
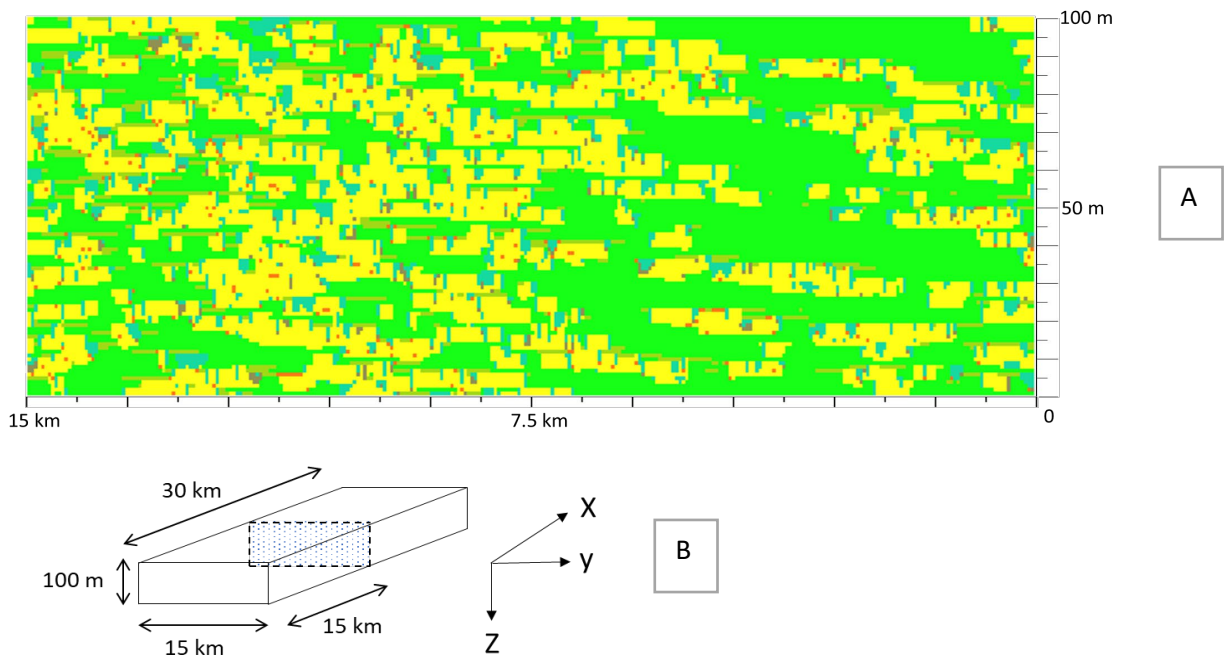
Figure 2.4: Run 1. Panel A shows a facies cross-section in the Z,Y-plane perpendicular to the flow direction from Run 1. As is shown in Figure 2.1, the yellow deposits are point bars, grey are sand plugs, orange are channel lags, green are floodplains, dark green are levees and turquoise are mud plugs. Panel B clarifies the position of the cross-section in the 3D block. As the only different input parameter between the runs, Run 1 uses a local avulsion period of 500 years. This results in a total N/G of this run of 36.3 %.
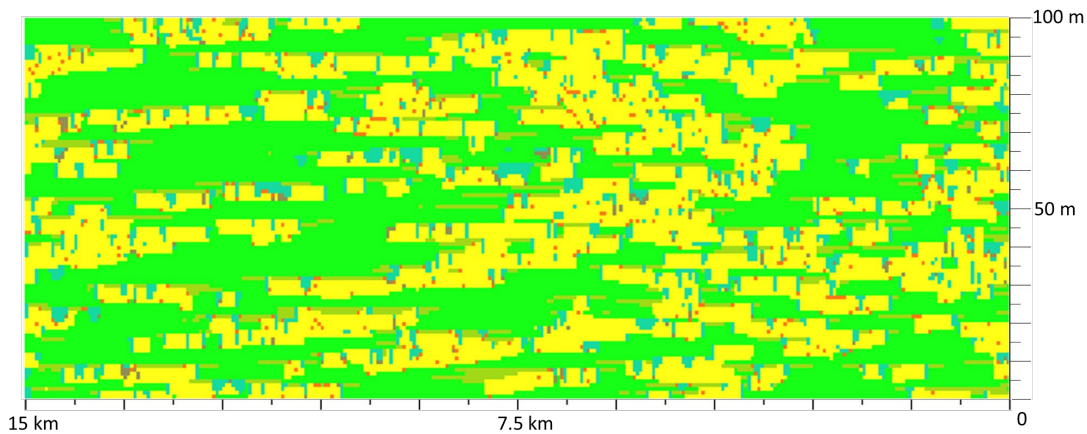
Figure 2.5: Run 2. A cross-section at the same position as shown in Figure 2.4B, with a local avulsion period of 1000 years. This results in a total N/G of this run of 37.6 %.
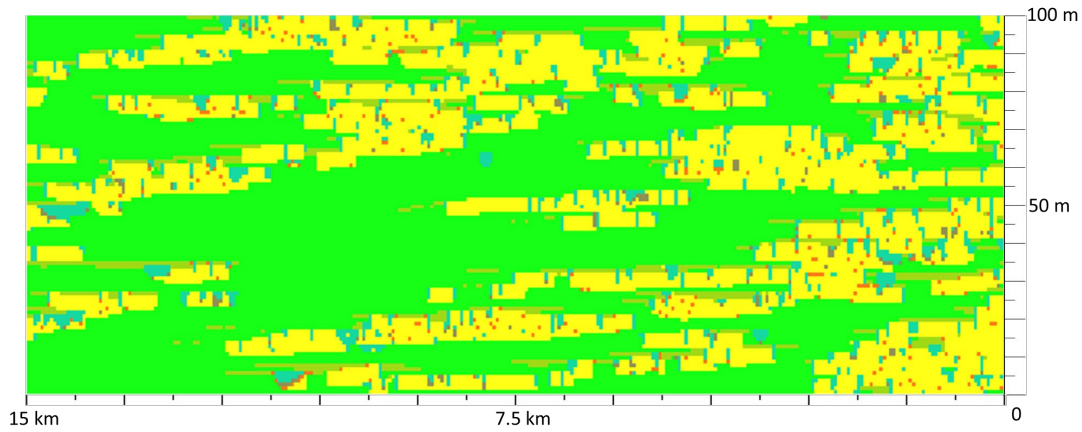
Figure 2.6: Run 3. A cross-section at the same position as shown in Figure 2.4B, with a local avulsion period of 1500 years. This results in a total N/G of this run of 32.1 %.
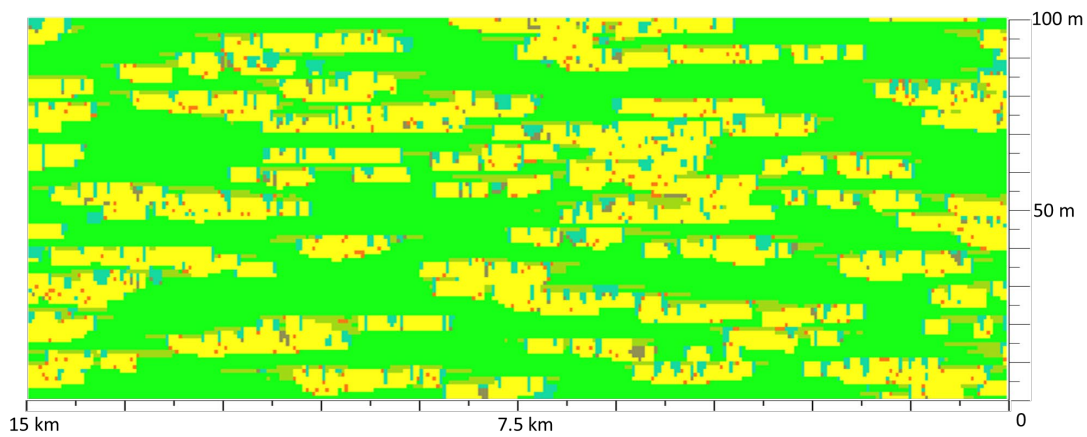
Figure 2.7: Run 4. A cross-section at the same position as shown in Figure 2.4B, with a local avulsion period of 2000 years. This results in a total N/G of this run of 32.4 %.
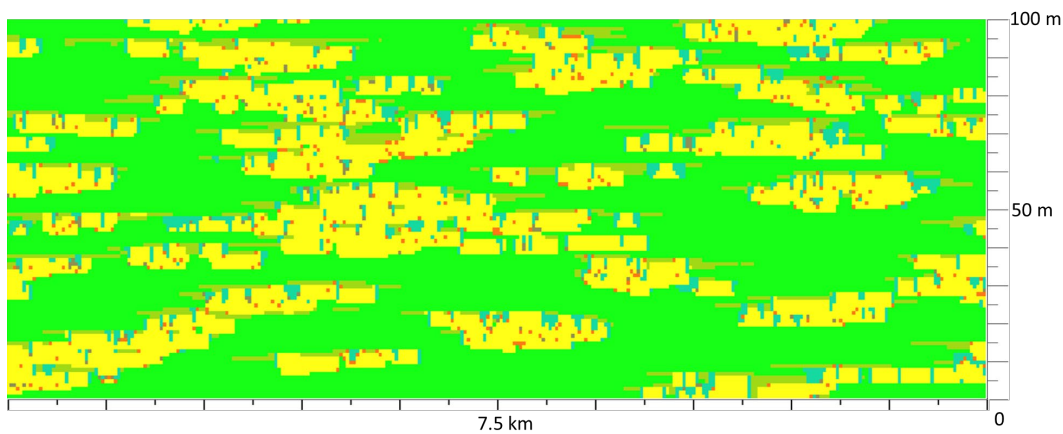
Figure 2.8: Run 5. A cross-section at the same position as shown in Figure 2.4B, with a local avulsion period of 3000 years. This results in a total N/G of this run of 28.4 %.
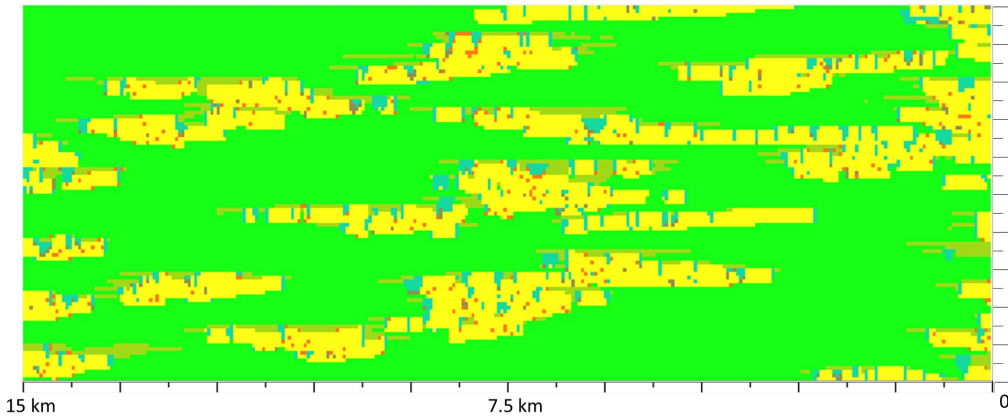
Figure 2.9: Run 6. A cross-section at the same position as shown in Figure 2.4B, with a local avulsion period of 4000 years. This results in a total N/G of this run of 24,6 %.
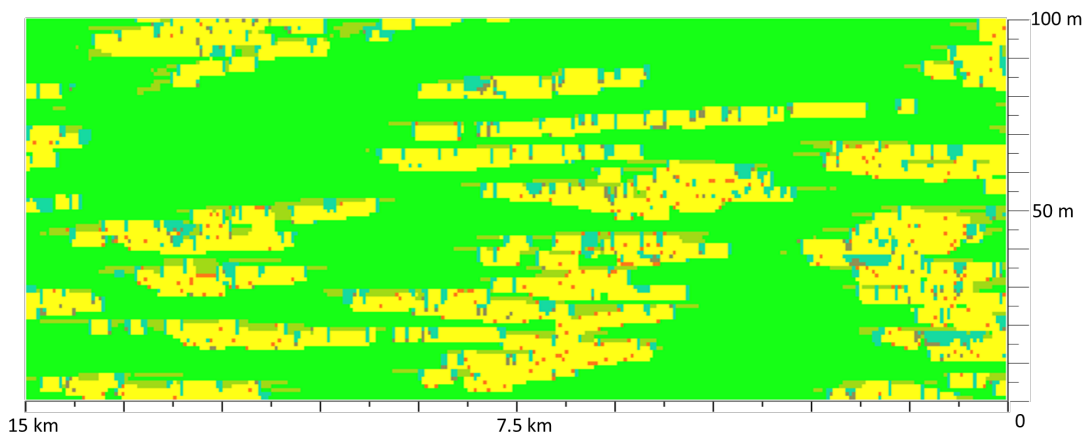
Figure 2.10: Run 7. A cross-section at the same position as shown in Figure 2.4B, with a local avulsion period of 5000 years. This results in a total N/G of this run of 23,4 %.
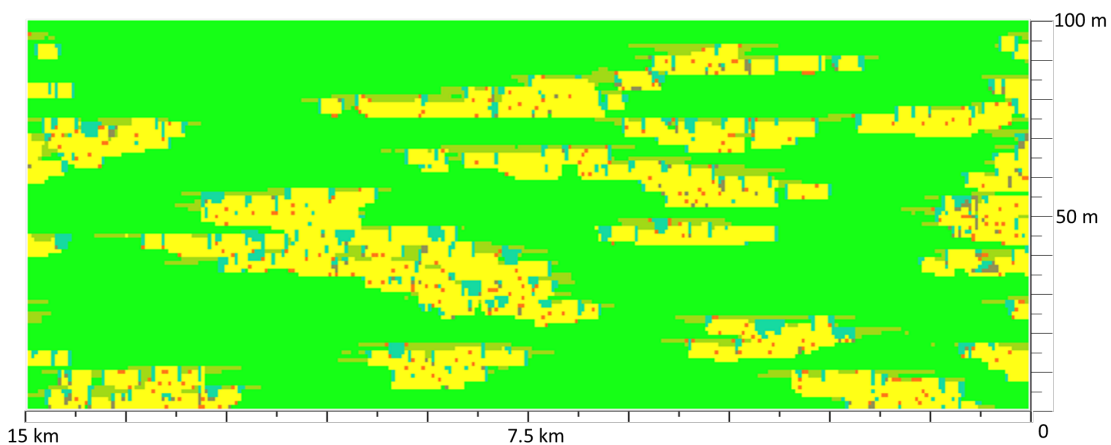
Figure 2.11: Run 8. A cross-section at the same position as shown in Figure 2.4B, with a local avulsion period of 6000 years. This results in a total N/G of this run of 25,0 %.

Maximum sediment thickness Flumy parameter test

The difference in regional and local avulsion periods is not the only difference between the non-cyclical and cyclical models. There is also a difference in the maximum sediment thickness Flumy parameter. This parameter controls the thickness of the floodplain deposits. As described in Table 2.5, the non-cyclical models have a uniform range of maximum sediment thickness between 0.2 and 0.6 m, while the cyclical models have a constant maximum sediment thickness of 0.2 m. This had to be done, since otherwise non-cyclical models would have far too much sand sediment deposited compared to the cyclical models and can not be properly compared. To test this, two non-cyclical models with a local avulsion period of 3000 years, same as non-cyclical Run 5 (Figure 2.8), were constructed with a constant maximum sediment thickness of 0.2 m. This is to show what would happen when this parameter was not changed. The first test is presented in Figure 2.12 and shows much more sand deposition, resulting in a N/G of 39,7 %, compared to the N/G of non-cyclical Run 5 of 28,4 %. The second test in Figure 2.13 again shows a similar picture, resulting in a N/G of 40,8 %.
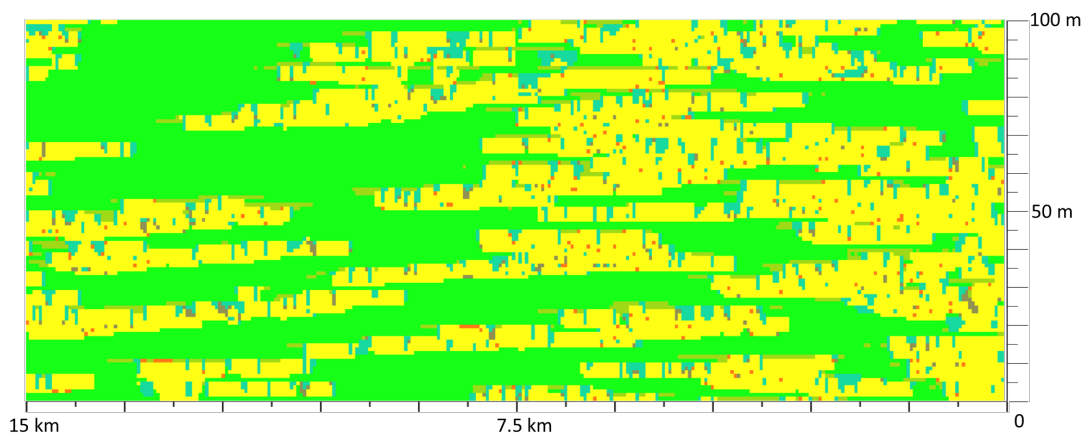
Figure 2.12: Maximum sediment thickness parameter test 1. A cross section at the same position as shown in Figure 2.4B. This non-cyclical run test has a local avulsion of 3000 years, the same as run 5 in Figure 2.8. The difference between run 5 and this run is that the maximum sediment thickness is now a uniform 0.2m. This results in much more sand deposited, giving a higher N/G of 39,7 %, compared to the N/G of run 5 of 28,4 %.
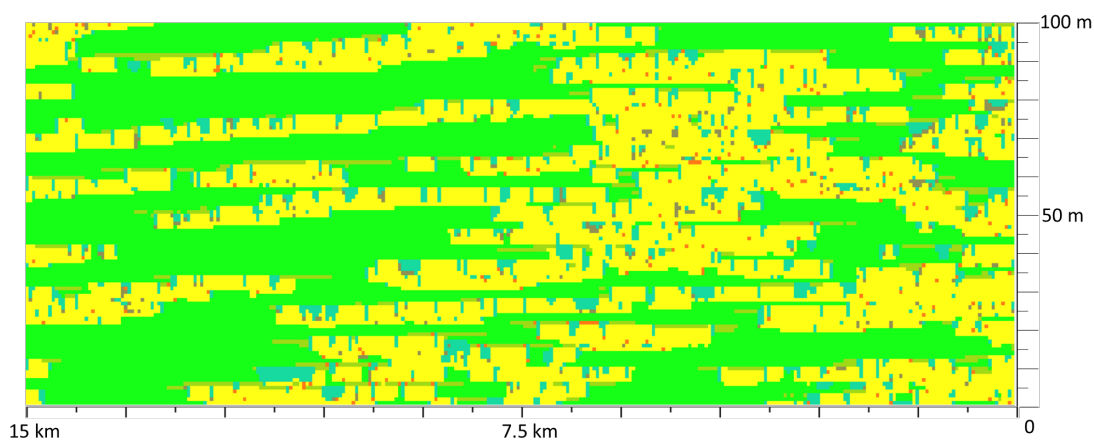
Figure 2.13: Maximum sediment thickness parameter test 2. A cross section at the same position as shown in Figure 2.4B. This non-cyclical run test has a local avulsion of 3000 years, the same as run 5 in Figure 2.8. The difference between run 5 and this run is that the maximum sediment thickness is now a uniform 0.2m. This results in much more sand deposited, giving a higher N/G of 40,8 %, compared to the N/G of run 5 of 28,4 %.

Non-cyclical model variability test

Non-cyclical Run 5 (Figure 2.8) was chosen for assessment and comparison using geothermal flow modelling. To test the variability in this run, 5 additional test model runs were constructed with identical input parameters to those of non-cyclical Run 5. The results are shown in the cross sections of Figure 2.14, 2.15, 2.16, 2.17 and 2.18. The N/G of all these test runs is presented in Table 2.8. The test figures show that the sand body stratigraphy is not overly different than the one presented in Figure 2.8 of non-cyclical Run 5. In every test cross section there are accumulated sand bodies present, similar to the original non-cycliclal Run 5. Also, there is not a big difference in N/G comparing the original non-cyclical run 5 to the five test runs, with the largest difference being 2.5%.

Test Run #	N/G	Figure
Original run 5	28,4	2.8
Test run 1	30,1	2.14
Test run 2	29,3	2.15
Test run 3	30,6	2.16
Test run 4	30,9	2.17
Test run5	30,3	2.18

Table 2.8: The comparison of the original non-cyclical run 5 (Figure 2.8) and five identical test runs. This was done to test the variability in the non-cyclical model. It shows that there is not a big difference in N/G comparing the original non-cyclical run 5 to the five test runs, with the largest difference being 2,5 %.
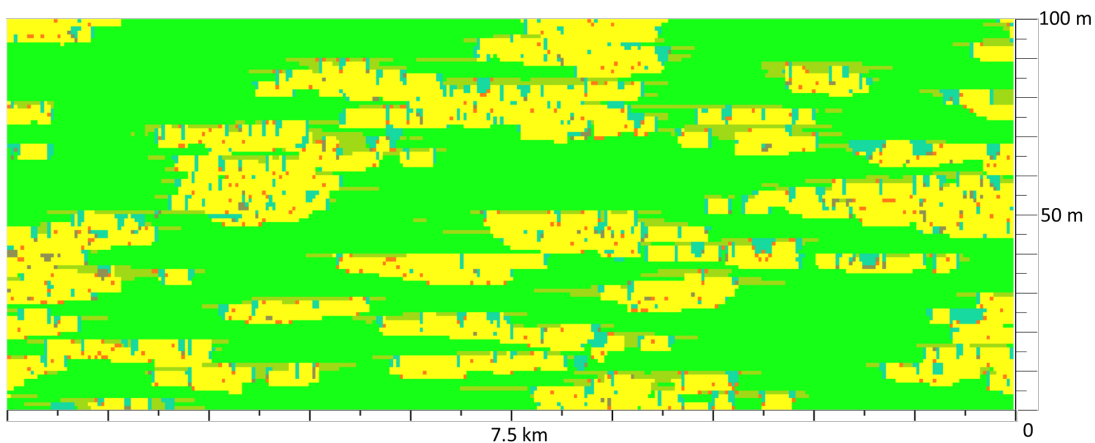
Figure 2.14: Test run 1. A cross-section at the same position as shown in Figure 2.4B. This test model run was constructed to test the variability in the non-cyclical model. It has identical input parameters to that of non-cyclical run 5 (Figure 2.8).
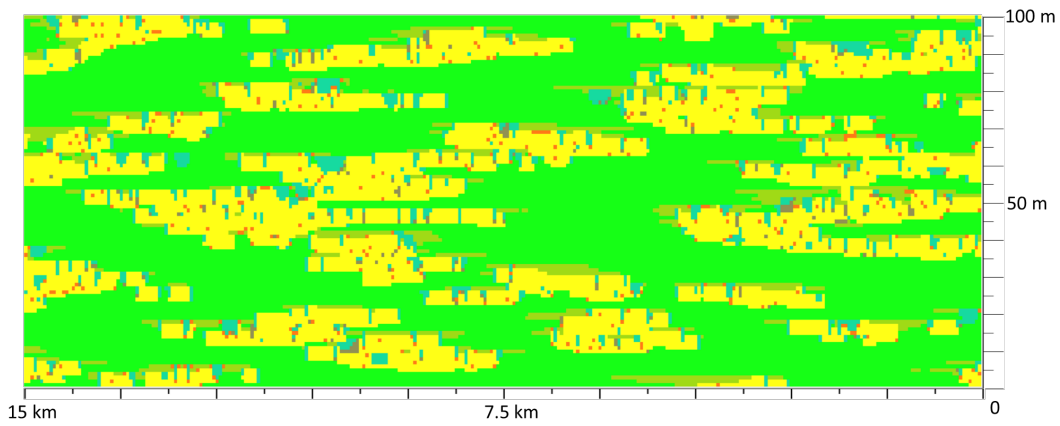
Figure 2.15: Test run 2. A cross-section at the same position as shown in Figure 2.4B. This test model run was constructed to test the variability in the non-cyclical model. It has identical input parameters to that of non-cyclical run 5 (Figure 2.8).
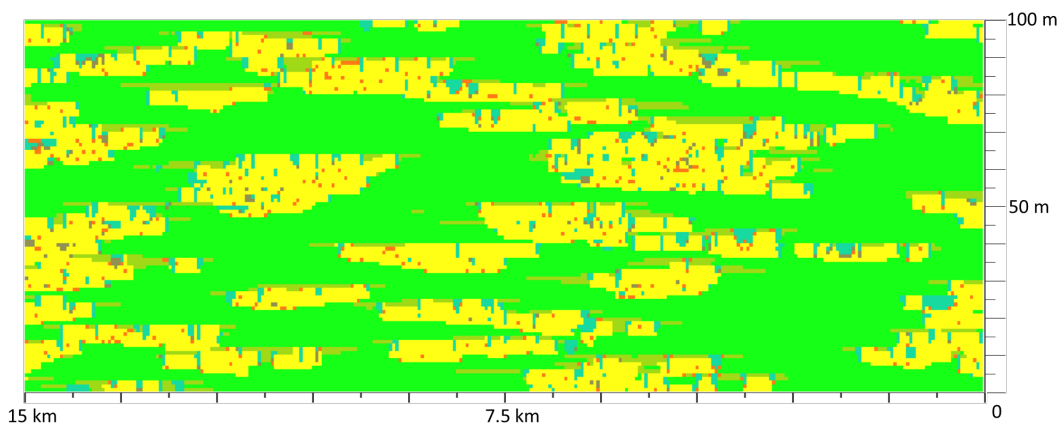
Figure 2.16: Test run 3. A cross-section at the same position as shown in Figure 2.4B. This test model run was constructed to test the variability in the non-cyclical model. It has identical input parameters to that of non-cyclical run 5 (Figure 2.8).
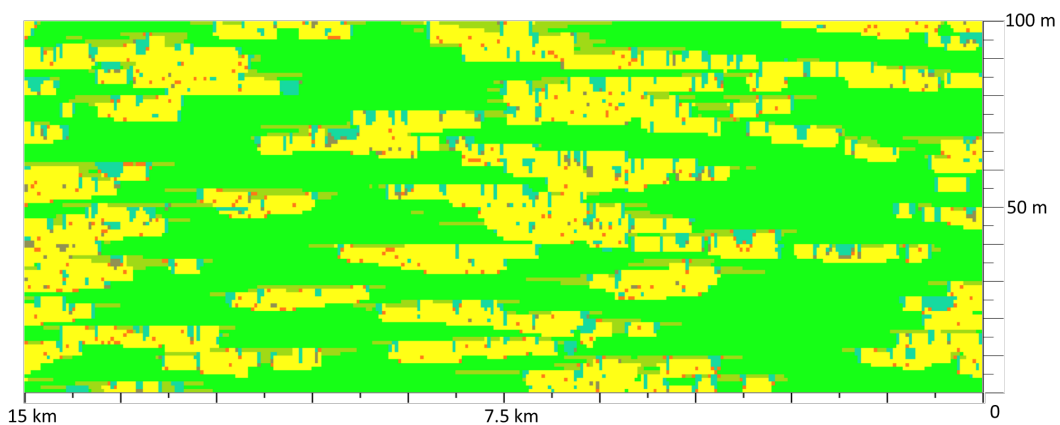
Figure 2.17: Test run 4. A cross-section at the same position as shown in Figure 2.4B. This test model run was constructed to test the variability in the non-cyclical model. It has identical input parameters to that of non-cyclical run 5 (Figure 2.8).
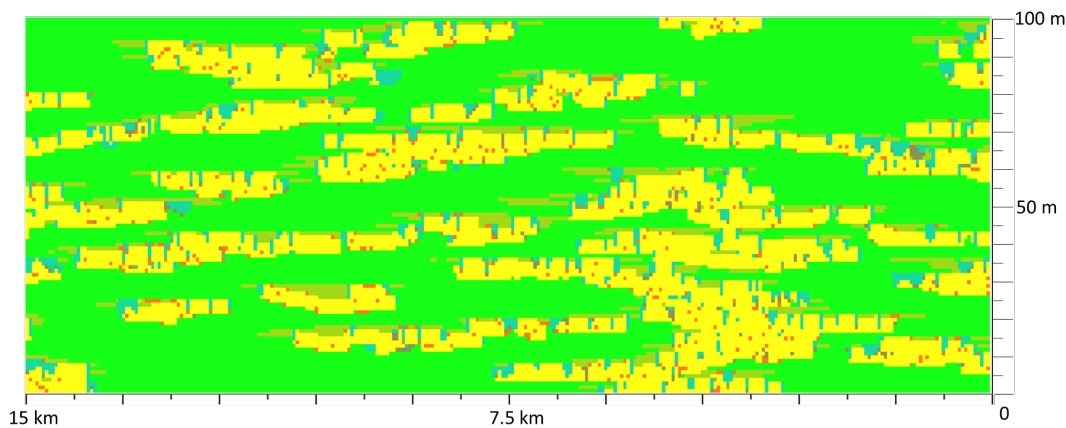
Figure 2.18: Test run 5. A cross-section at the same position as shown in Figure 2.4B. This test model run was constructed to test the variability in the non-cyclical model. It has identical input parameters to that of non-cyclical run 5 (Figure 2.8).

2.4.2 Cyclical runs

Two static hypothetical cyclical models were made. The input parameters for this type of model are given in Table 2.9. The parameters are chosen such that more cyclical behaviour occurs. Practically, this means that a certain rhythmic alternation of sand bodies (e.g. point bars, channel lag deposits) and clay floodplain deposits (e.g. mud plugs, overbank flooding deposits) is expected. This is replicated by simulating only a periodical regional avulsion similar to the precession Milankovitch cycle, and simulating no periodical local avulsion. The constructed cyclical models are hypothetical since only the regional avulsion period parameter is changed, with no local avulsion present. This is different in the cyclical models created in previous work by Abels et al, 2013 and Wang et al, 2021.

The two models have the exact same input parameters, see Table 2.9. There are only two differences. The first is that they were made with a different "seed". As was explained before, the simulation is stochastic and the seed value is used to generate the series of random numbers. Any realization of a simulation can be reproduced if the same seed value is taken when taking the exact same parameter values. The second difference is that the grid lag (grid cell size) was different. As illustrated in table 2.9 the grid lag for the first cyclic run was 30m, while for the second it was 50m. This means that the first cyclic run simulation has a higher resolution 3D block. For further reference, the two cyclic models are referred to as "*Cyclic Model 1*" and "*Cyclic Model 2*".

The difference in sand vs clay sediment deposited between *Cyclic Model 1* and 2 is minimal. To illustrate this, *Cyclic Model* 1 contained 27.4% sand and 72.6% clay. *Cyclic Model 2* contained 29.7% sand and 70.3% clay. The vertical thickness of the sand bodies were measured and from 25 measurements an average was taken, rounded to a whole meter. The observation is then that both models contain sand bodies of an average vertical thickness of 14m in *cyclic model 1* and 16m in *cyclic model 2*. This is fairly close to each other. There is a more significant difference in the range of the vertical thicknesses of the sand bodies. The minimum vertical thicknesses in both cyclical models are about 15 meters, while the maximum vertical thicknesses differs significantly. There is a higher maximum of about 40 meters in *Cyclic Model 1.* This in comparison with *Cyclic Model 2*, where the maximum vertical thickness is about 30 meters. This is all depicted and summarised in Table 3.6.

Cyclic Model #	Grid lag (input)	N/G	Sand body vertical thickness (average)	Sand body vertical thickness (range)
1	30m	27.4 %	14m	7 - 40m
2	50m	29.7 %	16m	6 - 30m

Table 2.9: The differences between hypothetical cyclic models 1 and 2 is illustrated. Cyclic Model 1 and Cyclic Model 2 have identical input parameters except that Cyclic Model 2 has a higher grid lag parameter. This means it has larger grid cells, which causes Cyclic Model 1 to have a higher resolution. The resulting output parameters are also displayed. These are the N/G, sand body vertical thickness (average) and the sand body vertical thickness (variation).

Connectivity

Another difference is the relative connectivity of the cyclic models. *Cyclic Model 1* seems to have more connected and accumulated sand bodies than *Cyclic Model 2*, while having almost the same N/G and similar sand body thicknesses. This can best be deduced when comparing the various cross sections in Figures 2.19 and 2.20. In Figure 2.19 a series of cross sections of *Cyclic Model 1* is illustrated in the z, y-plane, or "from the side". Where exactly the cross sections are taken in the 3D model is illustrated in Figure 2.19B. In the figure the sand deposits (mostly point bars) are shown in yellow, while the floodplain deposits are shown in light green. Figure 2.20 shows a series of cross sections taken from *Cyclic model 2*, which are taken at the same positions as in Figure 2.19. Especially the cross sections taken at the edges of the models (e.g. positions x = 0.01 km, x = 1 km, x = 27 km, x = 30 km) show a noticeable difference in the accumulation of the sand bodies. In *Cyclic Model 1* there are significantly more closely accumulated sand bodies. Notably, a visual comparison of connectivity is difficult to notice, which is why in Chapter 3 a more quantifiable expression of connectivity will be made using geothermal flow modelling.

X = 0.01 km   X = 3 km   X = 6 km

X = 9 km   X = 12 km   X = 15 km

X = 18 km   X = 21 km   X = 24 km

X = 27 km   X = 30 km

A

30 km

100 m

15 km

15 km

X

y

Z
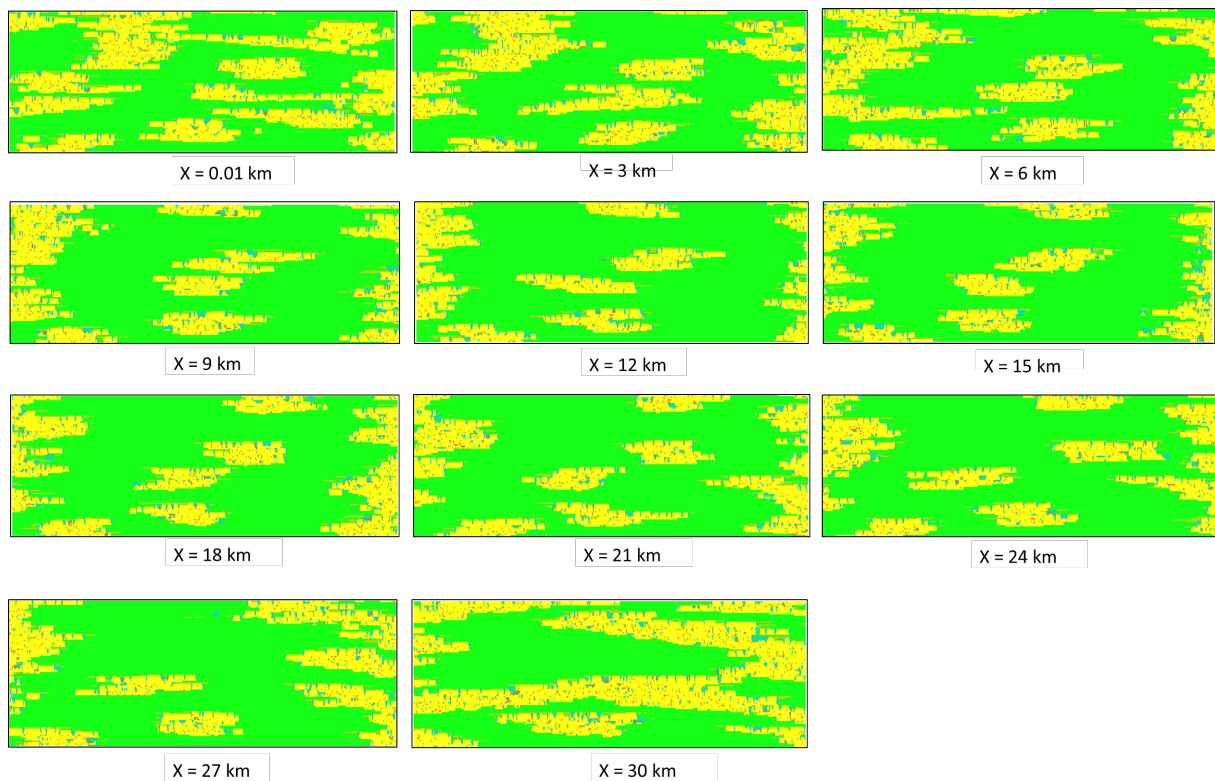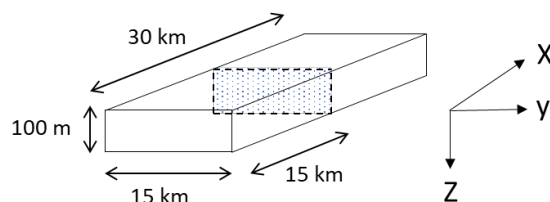
B

Figure 2.19: Cyclic model 1. Panel A shows multiple facies cross sections in the Z,Y-plane from Cyclic model 1. As is shown in figure 2.1, the yellow deposits are point bars, grey are sand plugs, green are floodplains, dark green are levees, turquoise are mud plugs, and orange are channel lags. From the top left cross section it goes downstream till it reaches the bottom right cross section. This is clarified in panel B. X = 0.01 km means it is most "east", while X = 30 km means it is most "west" and most downstream. It can be noticed how the connectivity changes when moving through the cross-sections. At X = 0.01 km the sand bodies are fairly connected, becoming less so e.g. X = 18 km. At X = 30 km the sand bodies become more connected again.
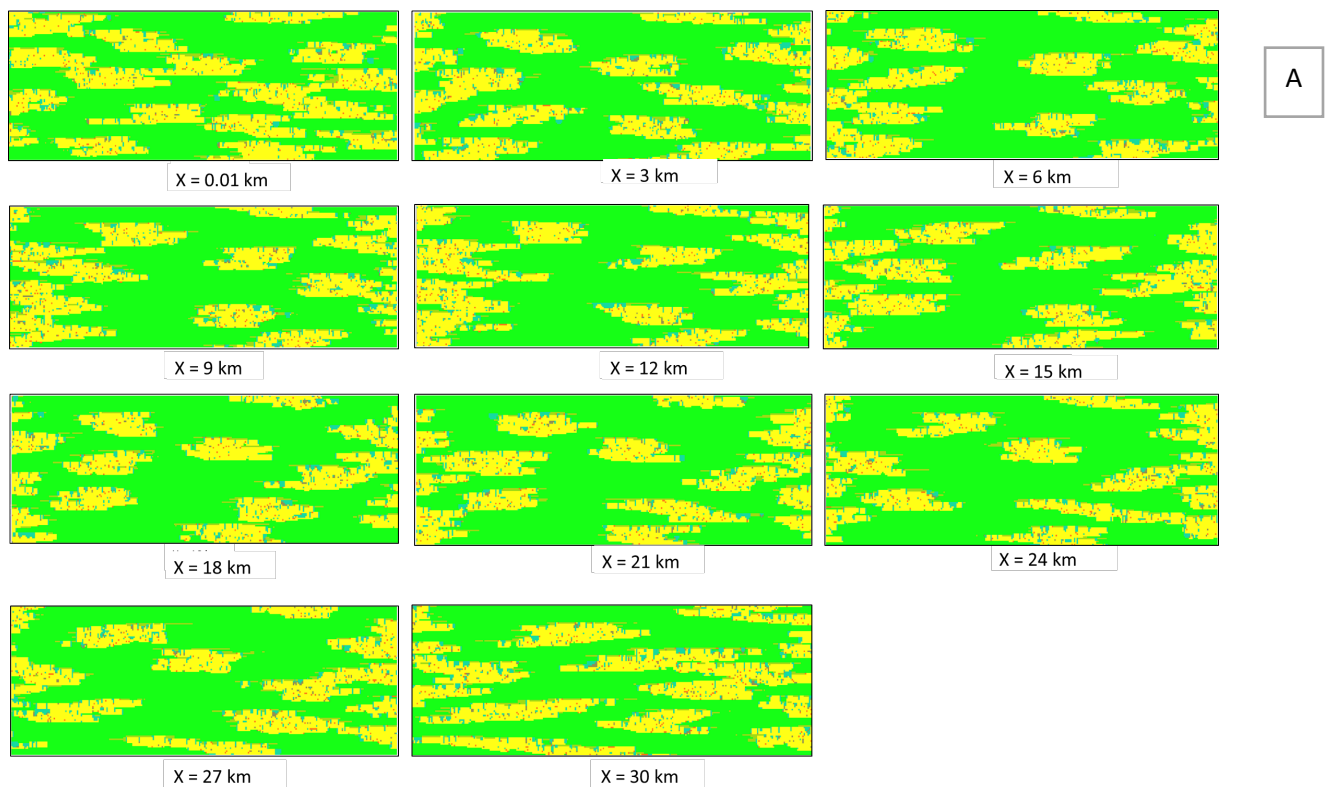
Figure 2.20: Cyclic model 2. Similar to Figure 2.19, Panel A shows multiple cross sections at the z, y plane from Cyclic model 2 moving downstream. Panel B has clarifications again for dimensions and the position of the cross sections. The connectivity changes again when moving through the cross sections. While overall there seems to be a bit less connectivity relative to Figure 2.19, there is still a decent amount. This can be seen at e.g. X = 0.01 km or at X = 30 km.

Depositional tendencies at the edges of the domain

Flumy deposits sediment inside the domain, but also (invisibly) deposits sediment outside the domain in the domain margin. This is illustrated in Figure 2.3. The reason for this is to remove border effects within the domain when the channel is migrating or aggradating. The default value for the domain margin equals 12 times the channel width and also corresponds to the development of at least one meander. Knowing this, a comparison can be made when looking at the tendency of sand bodies at the edges of the domain.

Cyclic Model 1 generally has more accumulation of sand bodies at the edges of the domain in comparison to *Cyclic Model 2*. This effect can be noticed when looking at the cross-sections discussed before in Figure 2.19 and Figure 2.20. It is determined from doing some sensitivity analysis that the cause of this seems to be random. However, this effect of stacking sand bodies at the edges of the domain seems to happens more often when the starting position (before any avulsion) of sand deposition is located near the edges of the domain. This is also what happened in *Cyclic Model 1*.

Deposition over time.

The fact that the starting deposition of sand deposition (mostly point bars) of *Cyclic Model 1* is near the edges can be deduced from Figure 2.21 and Figure 2.21. In these two figures of respectively *Cyclic Model 1* and *Cyclic Model 2* the deposition of the floodplains over time can be concluded. This is shown in the "B" panels. The darkest green floodplain deposits are first deposited and are therefore the oldest. The dark green becomes lighter and lighter, indicating the younger deposition. This option to show the lines and colour indications are extracted from an alternate visualization option in Flumy. From the "A" panels it can be hard to deduce at what order the yellow sand deposits are deposited. The order of deposition immediately becomes clear from the "B" panels.

A

15 km   7.5 km   0

B

15 km   7.5 km   0

C
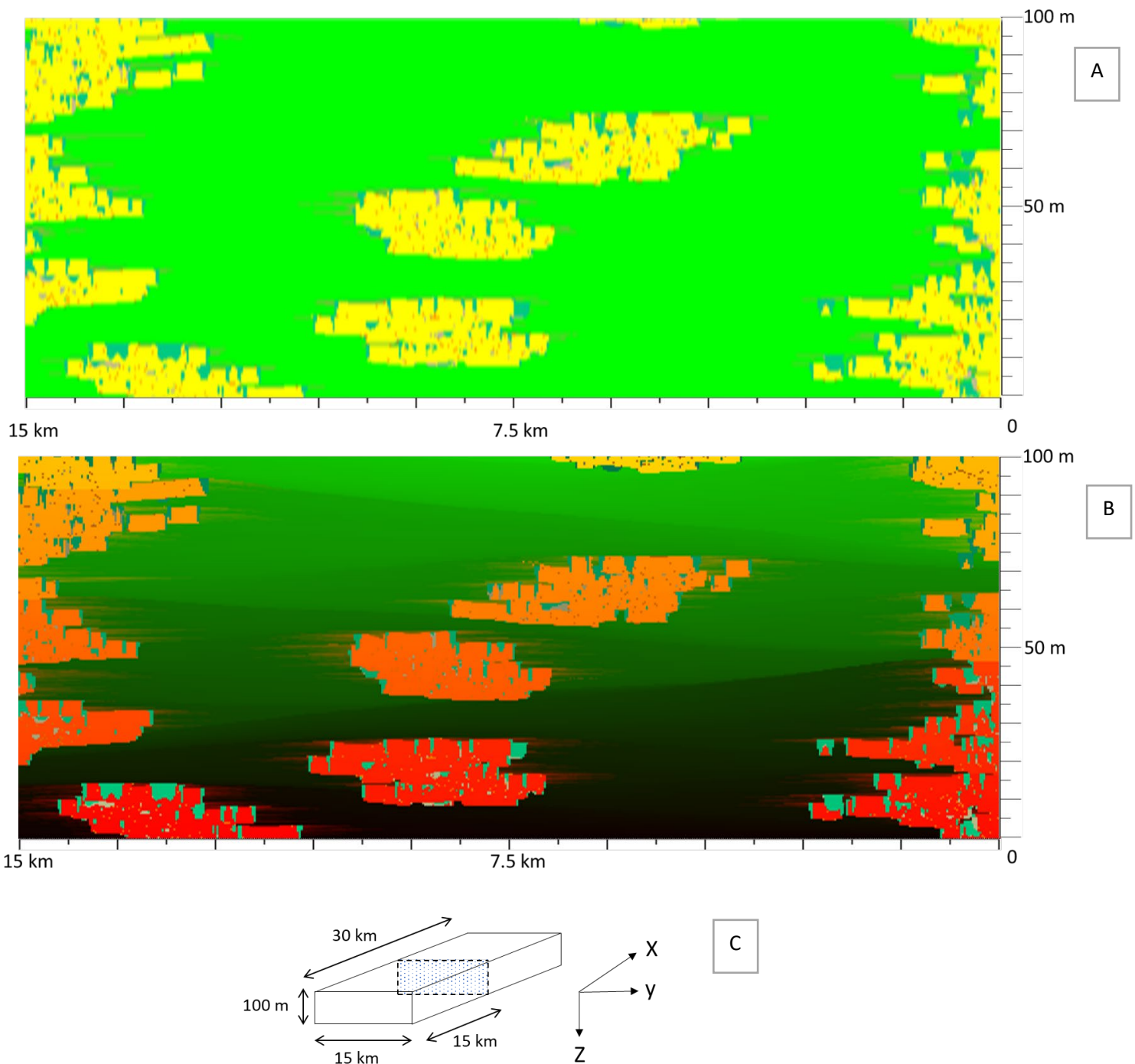
Figure 2.21: Cyclical model 1. A facies cross section in the Z,Y-plane, in the middle of the x-axis at position X = 15km from Cyclical model 1. Panel B represents a facies and age cross section at the same position. In this figure the red point bars are oldest, orange is younger, yellow is youngest. Panel C is a clarification of the dimensions of the 3D block and at which position the cross section is taken.
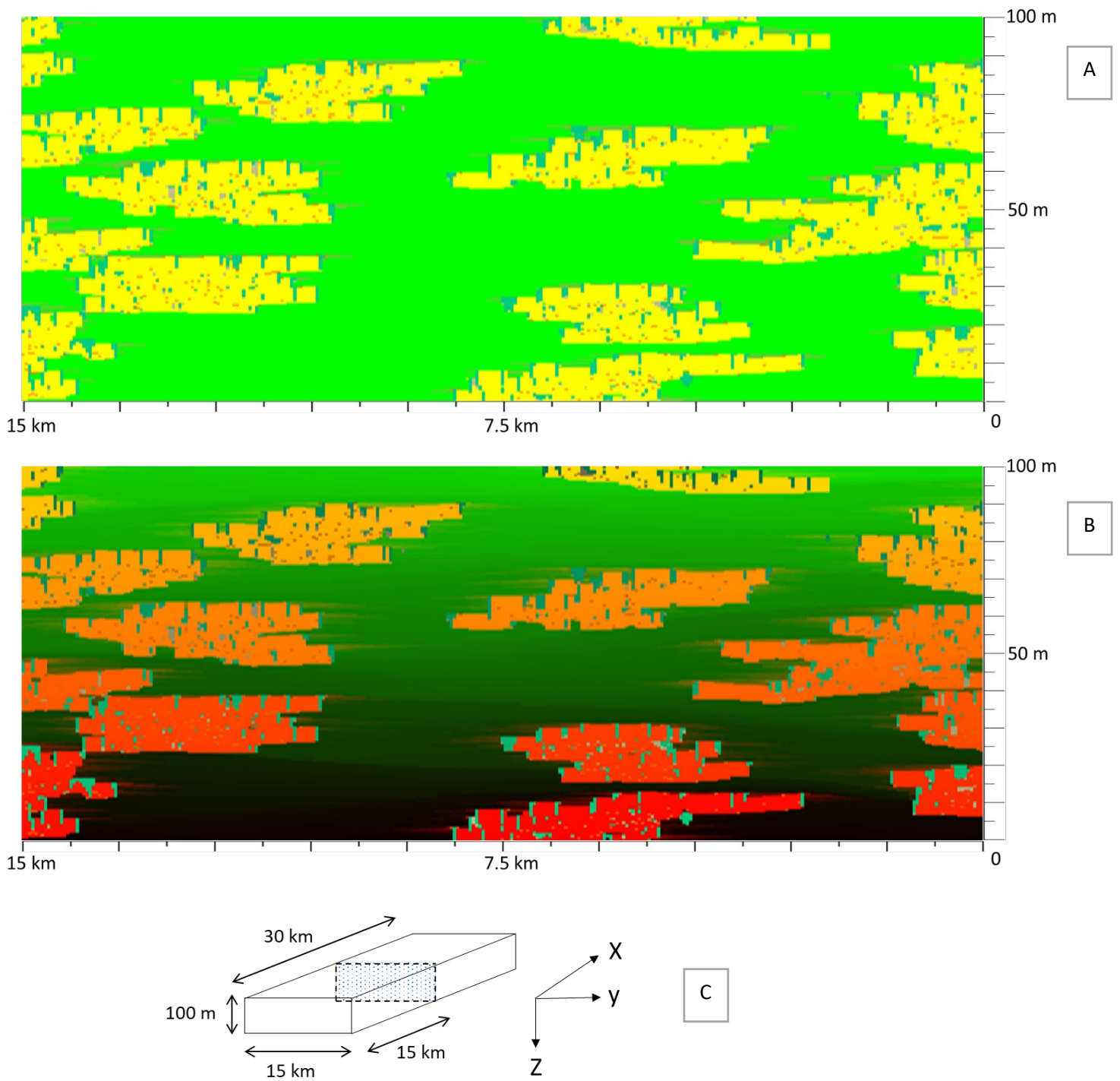
Figure 2.22: Cyclical model 2. Similar to Figure 3.11, although now the cross sections are taken from Cyclical model 2. Panel C again denotes the dimensions of the 3D block and at which position the cross section is taken.

3. Geothermal flow modelling

This chapter presents the DARTS geothermal modelling, done with one hypothetical cyclical model and one hypothetical non-cyclical model. First a brief introduction to DARTS is given in subsection 3.1 after which the workflow to the performed geothermal modelling is given in subsection 3.2. Concludingly, subsection 3.3 introduces the geothermal flow DARTS model simulation results. No sensitivity analysis is done involving DARTS, but a lot of sensitivity aspects are covered in the paper of Wang et al, 2019.

3.1 DARTS geothermal flow model

In this thesis Delft Advanced Research Terra simulator (DARTS) is used. This software is developed for various applications, of which a main use is geothermal reservoir modelling (DARTS, 2019). In subsections 3.1.1 and 3.1.2 the Operator-Based Linearization (OBL) approach is outlined, on which DARTS is based on. This OBL framework is used for complex multiphase flow and transport applications and seeks to improve to make the simulations run faster (Voskov, 2017) (Khait and Voskov, 2018a).

3.1.1 Governing equations and nonlinear formulation for two-phase geothermal simulation

The governing equations and nonlinear formulation for two-phase geothermal simulation with brine water can be described by the conservation of mass equation with n_p phases in (3.1) and the conservation of energy equation with n_p phases in (3.2).

$$\underbrace{\frac{\partial}{\partial t}\left(\phi \sum_{j=1}^{n_p} \rho_j s_j\right)}_{accumulation} - \underbrace{\nabla\left(\sum_{j=1}^{n_p} \rho_j u_j\right)}_{flux} + \underbrace{\sum_{j=1}^{n_p} \rho_j q_j}_{source/sink} \tag{3.1}$$

$$\underbrace{\frac{\partial}{\partial t}\left(\phi \sum_{j=1}^{n_p} \rho_j s_j U_j + (1-\phi)U_r\right)}_{Accumulation} - \underbrace{\nabla\left(\sum_{j=1}^{n_p} h_j \rho_j u_j\right)}_{\substack{heat\ transport \\ with\ fluid\ flux \\ (concection)}} + \underbrace{\nabla(\kappa\nabla T)}_{\substack{heat\ flux \\ (conduction)}} + \underbrace{\sum_{j=1}^{n_p} h_j \rho_j \widetilde{q}_j}_{source/sink} \tag{3.2}$$

where ϕ is porosity, ρ_j is phase molar density, s_j is phase saturation, U_j is phase internal energy; Ur is rock internal energy; h_j is phase enthalpy; u_j is the phase flux, κ is thermal conduction, T is the temperature and $\widetilde{q}_j$ is the source of phase (Wang et al, 2019) (Gries, 2015).

The saturation constraint is as follows with n_p phases:

$$\sum_{j=1}^{n_p} s_j = 1 \tag{3.3}$$

where S_j is the saturation in phase j.

Darcy's law is used as for a description of fluid flow in the reservoir:

$$u_j = K \frac{k_{rj}}{\mu_j} \left(\nabla p_j - \gamma_j \nabla D \right)$$

where u$_j$ is the phase flux, K is permeability tensor, k_{rj} is relative permeability for phase j, μ_j (3.4)
is phase viscosity, p_j is pressure in phase j, γ_j is gravity vector and D is depth (Wang et al, 2019) (Gries, 2015).

As mentioned before, pressure and enthalpy are chosen as primary variables in the nonlinear molar formulation (Wong et al, 2015) (Faust & Mercer, 1975).

Next, the Newton-Raphson method is employed to solve the linearized system of equations on each nonlinear iteration in this form:

$$J(\omega^k)(\omega^{k+1} - \omega^k) + r(\omega^k) = 0$$

(3.5)

where J is the Jacobian defined at the kth nonlinear iteration. The Operator-Based linearization (OBL) approach is applied in DARTS, which is explained next.

3.1.2 Operator-Based Linearization (OBL)

The OBL approach simplifies the programming code significantly, while still having enough flexibility and giving a higher performance. The architecture of the code also supports an extension to parallel computation and GPU programming (Khait & Voskov, 2017).

It OBL approach works as follows. The mass & energy conservation equations (3.1) and (3.2) are written in summative form. Then all variables in the equations are expressed as functions of a spatial coordinate ξ, and a physical state ω, except for the ones with the phase source terms (Wang et al, 2019).

The spatial variable ξ include the mesh geometry, permeability and porosity, and the physical state variable ω involve pressure, temperature (enthalpy) and composition. The state dependent operators f(ω) are the rock and fluid properties, determined at interface l. The space-dependent operators f(ξ,ω) create reservoir structure and heterogeneity (Wang et al, 2019) (Khait & Voskov, 2017).

The discretised mass conservation equation is as follows: (in operator form)

$$a(\xi, \omega)\left(a(\omega) - a(\omega_n)\right) + \sum_l b(\xi, \omega)\beta(\omega) + \theta(\xi, \omega, u) = 0$$

(3.6)

where ω and ω_n are the physical state of block i on the current and previous timestep respectively. $a(\xi, \omega)$, $\alpha(\omega)$, $b(\xi, \omega)$ and $\beta(\omega)$ are physical state dependent operators. These are described in equations (3.7), (3.8), (3.9) and (3.10). The porosity is assumed as a pseudo-physical state variable (Wang et al, 2019) (Khait & Voskov, 2017).

$$a(\xi, \omega) = \phi V$$

(3.7)

$$\alpha(\omega) = \sum_{j=1}^{n_p} \rho_j s_j$$

(3.8)

$$b(\xi, \omega) = \Delta t \Gamma^l \Phi_{p,ij} \tag{3.9}$$

$$\beta(\omega) = \sum_{j=1}^{n_p} \rho_j^l \frac{k_{rj}^l}{\mu_j^l} \tag{3.10}$$

$$\Phi_{p,ij} = \left(p_j + \gamma_p(\omega_j)\right) - p_i - \gamma_p(\omega) - \frac{\delta_p(\omega) + \delta_p(\omega_j)}{2}\left(D_j - D_i\right) \tag{3.11}$$

where ω_n is the physical state of block i in the previous timestep, ω_j is the physical state of block j, Γ^l is the transmissivity at interface l, p_j is phase pressure, $\gamma_p(\omega)$ is the capillary pressure operator for phase p, $\delta_p(\omega)$ is the density operator for phase p and D_j is the phase depth.

The discretised energy conservation equation is as follows: (in operator form)

$$a_e(\xi, \omega)\big(a_e(\omega) - a_e(\omega_n)\big) + \sum_l b_e(\xi, \omega)\beta e(\omega) + \sum_l c_e(\xi, \omega)\gamma_e(\omega) + + \theta_e(\xi, \omega, u) \tag{3.12}$$
$$= 0$$

Where ω and ω_n are the physical state of block i on the current and previous timestep respectively. $a_e(\xi)$, $a_e(\omega)$, $b_e(\xi, \omega)$, $\beta_e(\omega)$, $c_e(\xi)$ and $\gamma_e(\omega)$ are physical state dependent operators These are described in equations (3.13), (3.14), (3.15), (3.16), (3.17) and (3.18) (Wang et al, 2019) (Khait & Voskov, 2017).

$$a_e(\xi) = V(\xi) \tag{3.13}$$

$$a_e(\omega) = \phi\left(\sum_{j=1}^{n_p} \rho_j s_j U_j - U_r\right) + U_r, \tag{3.14}$$

$$b_e(\xi, \omega) = b(\xi, \omega) \tag{3.15}$$

$$\beta_e(\omega) = \sum_{j=1}^{n_p} \rho_j^l \frac{k_{rj}^l}{\mu_j^l} \tag{3.16}$$

$$c_e(\xi) = \Delta t \Gamma l (T^b - T^a) \tag{3.17}$$

$$\gamma_e(\omega) = \phi\left(\sum_{j=1}^{n_p} s_j \lambda_j - \kappa_r\right) + \kappa_r \tag{3.18}$$

In equation (3.17), T^b and T^a are assumed to be temperatures in neighbouring grid blocks a and b.

The representations in equations (3.6) and (3.12) simplify the complicated nonlinear physics significantly. This increases the performance significantly. The OBL framework proves to be accurate for various applications, flexible for complex extensions, highly efficient in terms of CPU and extendable to advanced architectures (Khait & voskov, 2018).

3.2 Methodology to geothermal flow modelling

The subsection describes the workflow for the analysis of the impact of different sandstone body stratigraphies in the hypothetical cyclical and hypothetical non-cyclical models on geothermal flow. These results are made through DARTS geothermal flow simulations.

Step 1.
The first step was to choose the hypothetical cyclical and hypothetical non-cyclical models which are to be compared. The selected models are non-cyclical run 5 (Figure 2.8) and cyclical run 2 (Figure 2.22). These were chosen since they have similar N/G. The total block of the non-cyclical run has a N/G of 28,4 %, while the cyclical run has a N/G of 29.7 %. Also the sand body thickness is no too far apart with the non-cyclical generally being around 12m, while the cyclical run being around 16m. The grid input lag is also 50x50m (X*Y) for both runs.

Step 2.
Before geothermal flow modelling can be done in DARTS, first the petrophysical properties need to be assigned to the chosen models in Matlab. These are the permeability and porosity of the different facies. All facies from the facies model generated from Flumy (Figure 2.2) are simplified into reservoir and non-reservoir units. The sandy facies are considered reservoir units and consist of point bars, channel lags and sand plugs. The shaly/silty facies are considered non-reservoir units and consist of crevasse splays, overbank deposits, levees and mud plugs.

All shaly non-reservoir units were considered to be homogeneous and nearly impermeable. The porosity was assigned to be 10% and the permeability assigned 5 mD (Willems et al, 2017). To make the sandy reservoir units heterogeneous and permeable a beta distribution correlation function was used to assign the porosity. The distribution was derived from core plug data from the West Netherlands Basin (WNB) in the Netherlands. This distribution was used because no data was available from the Bighorn Basin, thus this was the closest solution available. The distribution characteristics include a mean of 0.28, standard deviation of 0.075, skew 0.35 and kurtosis of 2.3 (Willems et al, 2017). The permeability of the reservoir units was derived from the following porosity-permeability relationship in equation (3.19). This relationship was produced from petrophysical data from well MKP-11, also from the WNB.

$$K = 0.0633\, e^{(29.507\varphi)}$$

$$(3.19)$$

where K = permeability(mD) and φ is porosity(-) (Willems et al, 2017). This porosity distribution creates a porosity range of 15-38%, while the porosity-permeability relationship establishes a permeability range of 6-3000 mD in the reservoir facies.

Step 3.
Overburden and underburden layers were created to add to the facies model. These were made to provide a thermal recharge. This means that the ambient temperature can slightly recover from the cooler water flow in the model. The over and under burden layers were both taken to be 200 m thick, while having homogeneously low values porosity and permeability of 5 % and 0.1 mD respectively. In Matlab the N/G can be derived since the percentages of sands and shales is known.

Step 4.
To undertake the analysis of the sand body stratigraphies it was decided to subsample the cyclical and non-cyclical models. The reason for this is that large static model inputs are difficult to handle and simulate in DARTS for any laptop or pc. It takes a very long time and it won't finish due to pressures getting out of control. Subsampling makes it possible to do DARTS geothermal simulations in a relatively short time while still getting relevant results to compare the models.

First an area inside the total models of the cyclical and non-cyclical model was chosen from which within the subsamples were constructed. This area ended up to be 10 km in the X-direction, 9,5km in the Y-direction and 60 m in the vertical Z-direction for both models. These smaller areas are big enough such that is possible to compare the variability in the total models. These areas' dimensions are visible in Table 3.1, as well the dimensions of the subsamples. Table 3.2 shows the exact locations of these areas within the total models.

Parameter		Total model	Area inside total model used for subsampling	Subsamples
Reservoir dimension (grid size)	X-axis (km)	30km	10km	2,5km
	Y-axis (km)	15km	9,5km	1,5km
	Z-axis (m)	100m	60m	60m
Grid dimension (# of grid cells)	X-axis (-)	600	100	50
	Y-axis (-)	300	120	30
	Z-axis (-)	100	60	60
Grid block size	X-axis (m)	50m	50m	50m
	Y-axis (m)	50m	50m	50m
	Z-axis (m)	1m	1m	1m
N/G (%)	Cyclical	29,7 %	n.a.	*10-40 % (variable)*
	Non-cyclical	28,3 %	n.a.	*10-40 % (variable)*

Table 3.1: Dimensions of the identically sized chosen areas inside the total model from the total cyclical and non-cyclical model. From these areas 55 subsamples were created for each cyclical and non-cyclical model. Only subsamples with a N/G of between 10 and 40 % were considered.

Parameter		[Cyclical model] Location of the area inside total model used for subsampling	[Non-cyclical model] Location of the area inside total model used for subsampling
Reservoir dimension (grid size **range**):	X-axis (km)	15 – 25 km	15 – 25 km
	Y-axis (km)	4,5 – 14 km	4,5 – 14 km
	Z-axis (m)	20 – 80 m	20 – 80 m

Table 3.2: Showcasing the difference in location of the chosen smaller blocks in the cyclical and non-cyclical models. There is only a difference in location in the Y-axis. This was needed for both chosen smaller blocks to have similar N/G.

These areas inside the total models were chosen away from the edges, away from any possible boundary effects. A boundary effect is especially visible in the cyclical model, while the non-cyclical model has this to a lesser extent. This can be as observed in Figure 3.1, which portrays cross sections of the cyclical and non-cyclical models at the X-plane. When considering the X-direction, the areas were chosen at 15-25 km from a total 30km. This is sufficiently downstream as seen in Figure 3.2, such that is away from the area at which the channels originate. This is especially visible in the non-cyclical model in Figure 3.2B, since it has no regional avulsion and only local avulsion occurs. It was also taken into consideration to choose areas which contained appropriate amounts of sand vs clay. Areas of only clay are not possible to simulate since the water wouldn't have enough of a connection from injector to producer well and the pressure build-up would become too much.

55 subsamples were sampled in each of the cyclical and non-cyclical models with dimensions of X = 2,5 km, Y = 1,5 km and Z = 60m. Where possible, the subsamples are half overlapping in the discussed allocated areas. Only subsamples were taken with a N/G of between 10 and 40 %, see Figure 3.1. Subsamples with a too low N/G don't give a breakthrough time and subsamples with too high N/G don't give us enough information about model differences. The geothermal flow modelling was exclusively done on the subsamples.
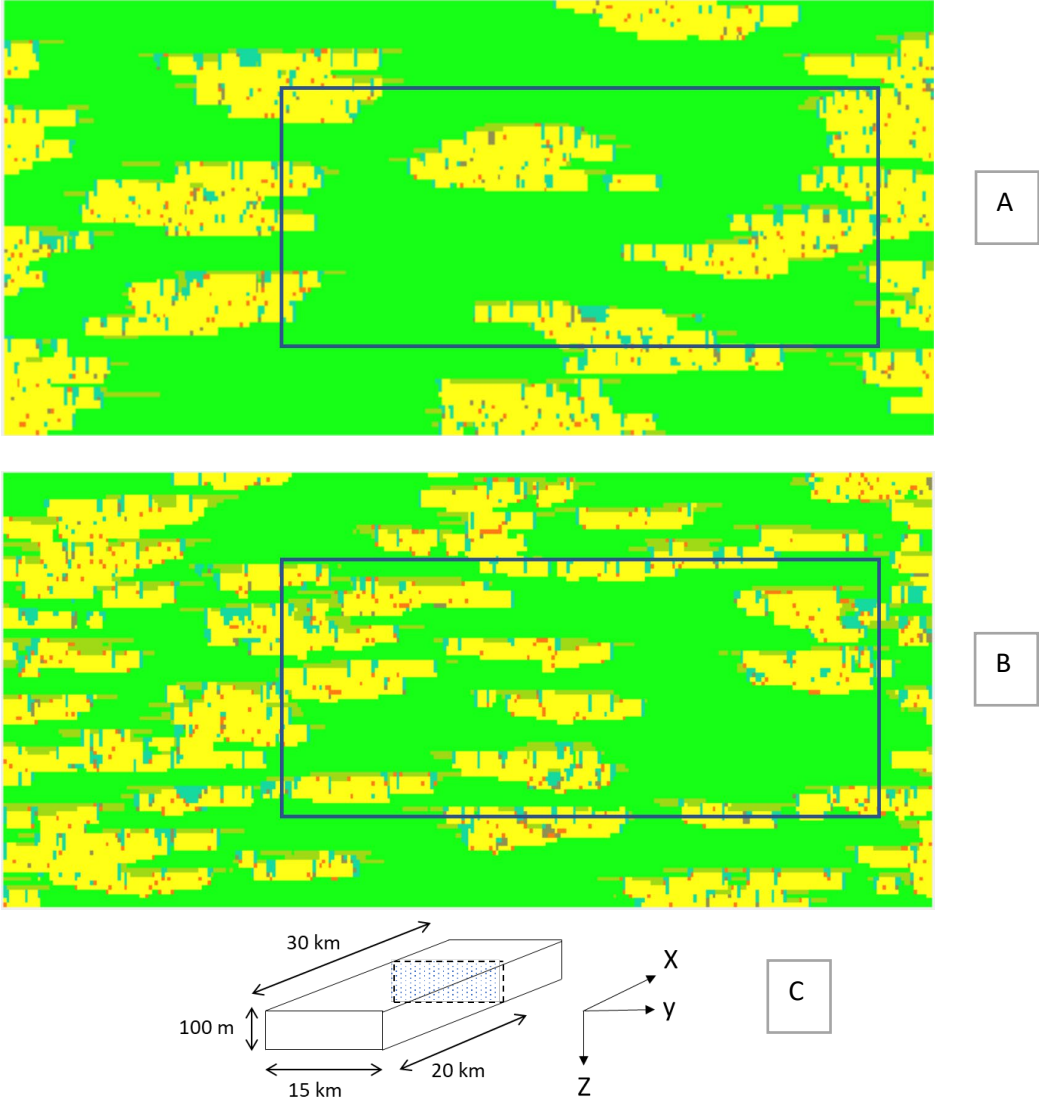
Figure 3.1: Portraying the position of the smaller chosen block in the models in example cross-sections, visualized in Petrel. Panel A is a cross-section of the cyclical model in the X-plane at X=20 km. Panel B contains a cross-section of the non-cyclical model in the X-plane, also at X=20 km. The position of the cross-sections in the total model is visualized in Panel C.
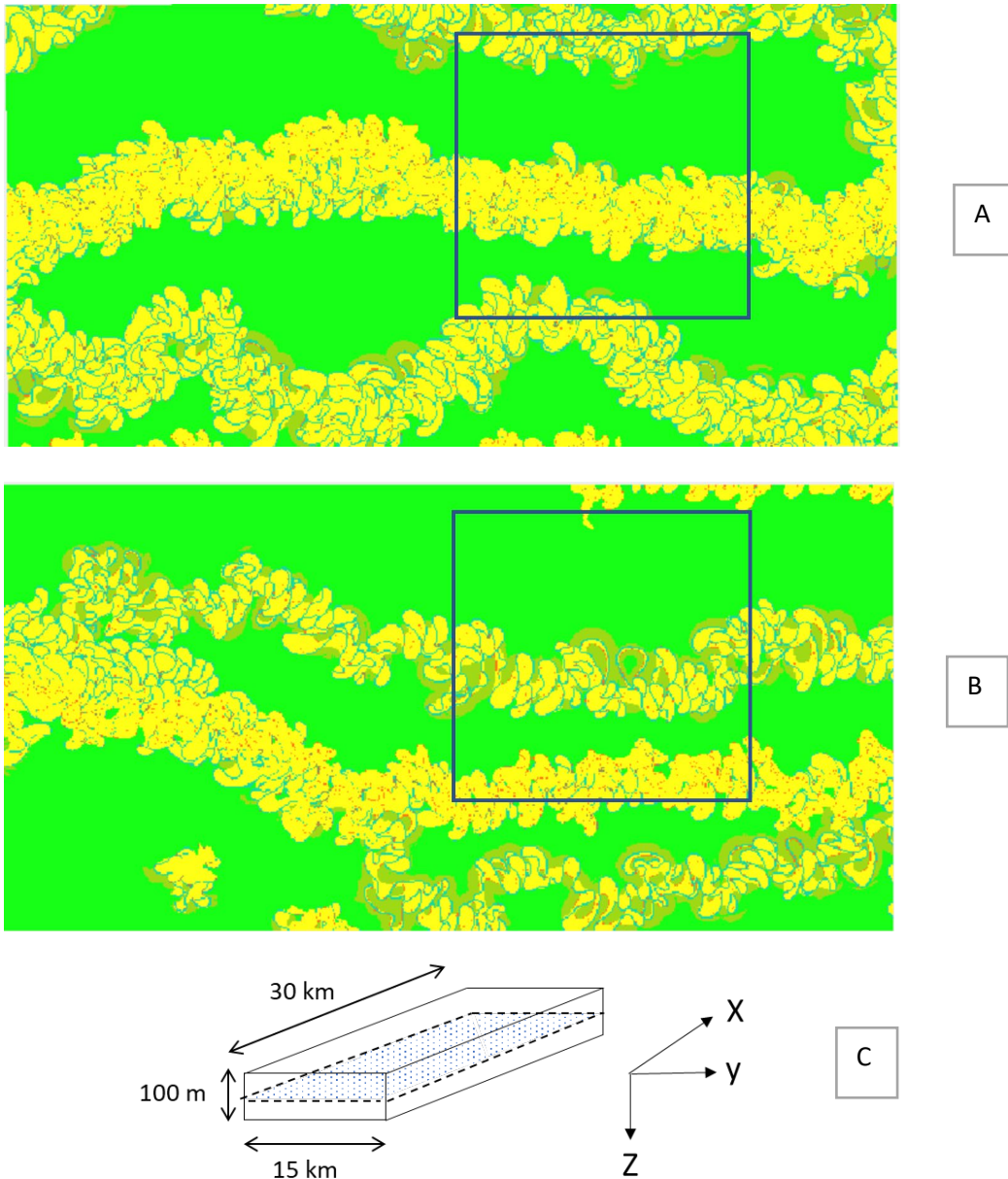
Figure 3.2: 40m. Portraying the position of the smaller chosen block in the models in example cross-sections, visualized in Petrel. Panel A is a cross-section of the cyclical model in the Z-plane at X=40 m. Panel B contains a cross-section of the non-cyclical model in the Z-plane, also at X=40 m. The position of the cross-sections in the total model is visualized in Panel C.

Step 5.
After selecting the subsamples the input parameters for the DARTS simulations were chosen. One injector and one producer well were put into each of the subsamples. These well doublets were needed for the flow to occur from injector to producer well.

The subsample simulations were made with both a BHP control and water rate control. BHP means bottom hole pressure, or pressure at the well. Only one of these controls can be used at the same time and they produce very different results. When using the BHP control in simulations a constant pressure is set in the injector and producer wells. This is not changed for the entire simulation. There must be a pressure difference in the wells for the water to flow from injector to producer. When using water rate

control as a control in the simulations a fixed water flow rate is set. This fixed water rate is the same for the producer and injector and stays the same over the whole simulation.

Looking over at Table 3.3, first of all the run time in all of the subsamples was chosen to be at 35.000 days or about 96 years. This run time was chosen to have stable simulations while still having enough time to get useful results. Specifically the water rate control simulations have problems in this regard. For the water rate control sometimes there is a narrow window in which they work, outside of this window no useful results are created or the pressure inside the reservoir blows up.

The initial reservoir pressure in the subsamples is chosen at 200 Bar and the initial reservoir temperature is at 348,15 K. All layers are penetrated except for the overburden and underburden present above and below the subsamples.

Regarding the BHP control simulations, the BHP is set to 205 Bar at the injector well and 195 Bar at the producer well. When using the water rate control, the rate is set at 500 m^3/day for both the injector and producer wells. The well locations inside the subsamples are set to be precisely in the middle, with a distance of 1 km between the injector and producer well.

Parameter		Subsample
Run time (days)		35k days / ~96 years
Initial pressure (bars)		200 bar
Initial temperature (K)		348,15 K
Over/underburden		Yes
Layers penetrated		All except OB/UB
Time step (max) (days)		365 days
Heat capacity kJ/day/(m*K)		2200 kJ/day/(m*K)
Conductivity kJ/(m^3*K)		100 kJ/(m^3*K)
Boundary conditions		*Closed boundary*
Well parameters:	Control type injector well	BHP/Water rate
	Control type producer well	BHP/Water rate
	Initial T injection well (K)	308,15 K
	BHP injector well (Bars)	205 Bar
	BHP producer well (Bars)	195 Bar
	WR injector (m3/day)	500 m^3/day
	WR producer (m3/day)	500 m^3/day
Injector and producer relative well locations		Located directly in the middle of the subsample, 1 km distance between injector and producer)

Table 3.3: Darts input paraters and well locations explained for the subsample simulations. When using BHP control, the injector is set at 205 Bar while the producer is set at 195 Bar. When the water rate control is used, the rate is set at 500 m^3/day for both the injector and producer wells. The well locations are set precisely in the middle of the subsalmples, with 1 km distance between injector and producer.

Step 6.
Many different results can be attained from the geothermal flow simulations. Specifically the results which are relevant to analyzing sandstone body stratigraphies were taken. These results allow us to analyze connectivity, flow paths between wells and possible temperature exchanges between sand and clay bodies. Also it is analyzed if outliers in the subsample simulations make sense. The difference between BHP and water rate controlled simulations is also discussed. Each of these results are compared to the cyclical and non-cyclical subsample models.

The breakthrough time in the geothermal simulation of all the subsamples was determined. This is the time at which the colder water from the injector well reaches the producer well. Or in other words it is the time at which the producer well temperature falls under the initial reservoir temperature. In all of our simulations this initial temperature is taken at 348,15 K (Table 3.3).

For both the BHP and water rate control the subsample N/G is set out against the breakthrough time Also the subsample N/G is set out against the BHP/water rate difference at a specific fixed point in time in the simulations. This BHP/water rate difference is done by subtracting the BHP or water rate, depending on the control used, of the injector minus the producer well. First sufficient time needs to pass to reach steady state in the flow simulation, that's why it can't be taken at the start. The BHP/water rate difference is taken from each subsample simulation at 10.3k days specifically. It could not be taken at precisely 10k days since the simulation has a time step of 365 and only at each time step simulation data is provided. Lastly the producer temperature is set out against the breakthrough time to create a graph of temperature breakthrough curves.

Step 7.
The N/G set out against the breakthrough time at water rate control gives us the most intuitive information. This is why some extra statistical analysis was carried out over this graph. Specifically the breakthrough time mean and standard deviation of different N/G intervals were determined.

The sample standard deviation with Bessel's correction was used, since data is taken from subsamples and not the total population. This is captured in equation (3.20).

$$s = \sqrt{\frac{1}{N-1} \sum_{i=1}^{N} (x_i - \overline{x})^2} \qquad (3.20)$$

Where s is the sample standard deviation, N is the number of samples, x_i is the sample breakthrough time in this case, and $\bar{x}$ is the mean of the sample breakthrough times (Duncan, 1979).

3.3 Dynamic modelling results
In this section the geothermal flow modelling results are presented using DARTS. Using one chosen hypothetical non-cyclical model and one hypothetical cyclical model geothermal flow simulations were conducted after which they were compared.

As discussed before in subchapter 3.2 the selected models are non-cyclical run 5 (Figure 2.8) and cyclical run 2 (Figure 2.22).

Results that are relevant to analyzing sandstone body stratigraphies in the cyclical and non-cyclical models were taken. These include results to analyze connectivity, flow paths distances from injector to producer and possible temperature exchanges between sand and clay bodies. Outliers in the data are explained and differences between BHP and water rate controlled simulations are presented. All the results are compared between the cyclical and non-cyclical models.

3.3.1 Water rate control simulation results

First the geothermal flow simulation results using a fixed water rate control are presented using the subsampling method explained in the methodology (Table 3.1). It should be noted that using water rate as a well control as opposed to BHP produces results closer to how it is in reality. This is because in reality geothermal doublets are also controlled through the water flow rate.

N/G set out against BHP at the 10,3k simulation time step

First the subsample simulation results for the hypothetical cyclical and non-cyclical models are set out with the N/G values vs the BHP difference at a specific fixed time step in the simulation (Figure 3.3). This time step is taken at 10,3k days, since first a moment has to pass to reach steady state in the flow simulation. Taking the BHP differences of all subsample simulations at a specific time step allows us to easier compare the pressure at the wells (BHP) in the subsamples. The orange dots in Figure 3.3 are from the cyclical subsamples, while the blue dots are from the non-cyclical subsamples.

Looking at Figure 3.3 it is determined that generally a lower N/G means a higher BHP difference. This is logical since a lower N/G, which means less reservoir space, gives a higher resulting pressure difference while maintaining a fixed water rate. This trend is especially visible in subsamples of a N/G of between 20 and 40 %. In subsamples with a N/G below 20 % this relation seems to flatten, which means the BHP difference is not as closely tied to the N/G of the subsample anymore. The scatter is also the largest in subsamples with a N/G of below 20 % as well as having the most amount of outliers present.

Regarding the subsamples with a N/G of between 20 and 40 %, the cyclical and non-cyclical subsamples give a consistently similar trend, with little scatter and few outliers. The hypothesis is then that the connectivity of the subsamples in that range must also be similar.
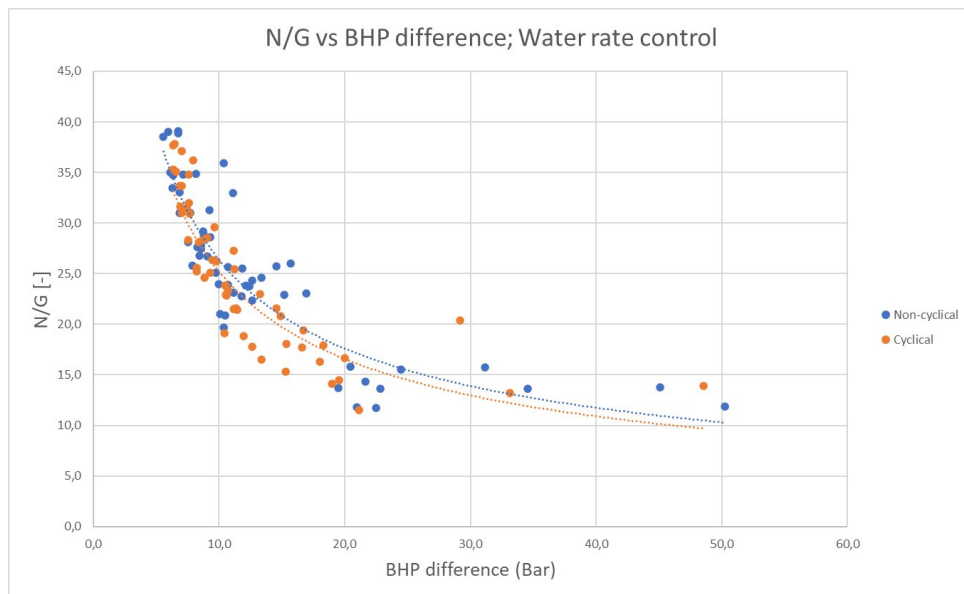
Figure 3.3: Simulation results of the cyclical and non-cyclical subsamples. The blue dots are non-cyclical subsamples, while the orange dots are cyclical subsamples. Using water rate as a well control N/G is plotted vs BHP at the producer well at a specific fixed time step in the simulation. This time step is taken at 10,3k days.

N/G set out vs breakthrough time

Next the hypothetical cyclical and hypothetical non-cyclical subsamples are set out with their N/G vs the observed breakthrough times (Figure 3.4). The orange dots in figure 3.4 are from cyclical subsamples, while the blue dots are from non-cyclical subsamples. The figure shows that generally a lower N/G, so a lower sand percentage relative to clay, gives a faster breakthrough time. This trend is logical since a low N/G means there is less sand volume for the water to flow through and thus the water reaches the production well faster, giving a faster breakthrough time.

There is plenty of scatter present as well as many outliers. It is visible that different N/G intervals give different results in Figure 3.4. The different N/G intervals are visualized with a dotted black line. It seems that especially between 20 and 30 % N/G, the non-cyclical subsamples have a generally equal or slower breakthrough time compared to the cyclical subsamples.
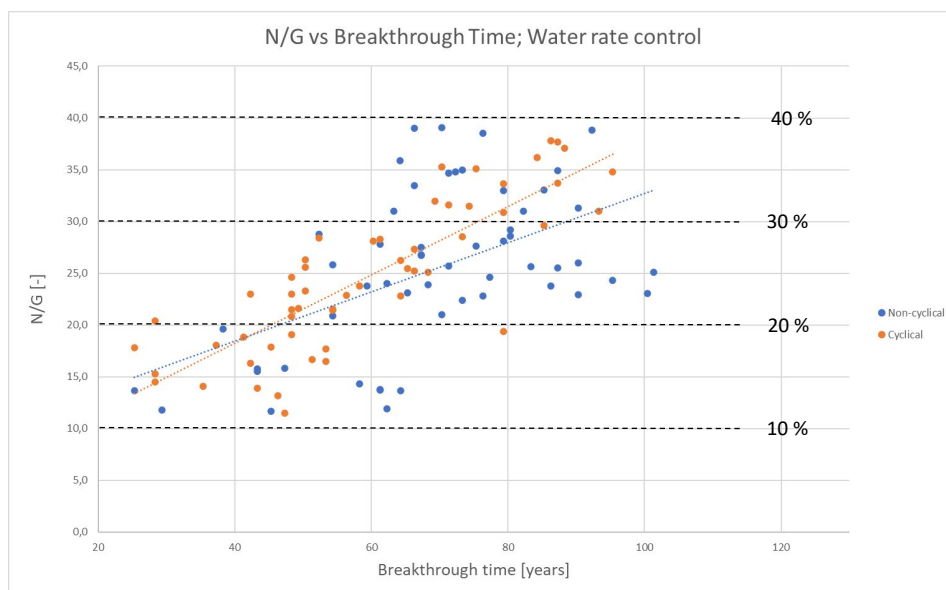
Figure 3.4: Breakthrough time set out against N/G. The orange dots are cyclical subsamples, while the blue dots are non-cyclical subsamples. The subsamples are divided up into N/G intervals. It is especially visible that the subsamples with a N/G of between 20 and 30 % give an equal or slower breakthrough time compared to the cyclical subsamples.

Considering the hypothesis that the connectivity is similar, it creates the impression that it is not the connectivity between the non-cyclical and cyclical model that makes the difference in the 20-30 % N/G interval, but a difference in flow path length between injector and producer well. When comparing a cyclical and non-cyclical subsample with similar N/G in this interval, it seems that the length of the flow path is equal or shorter for the cyclical model compared to the non-cyclical model, while having similar connectivity. This new hypothesis creates the impression that it is not the connectivity between the non-cyclical and cyclical model that makes the difference, but a difference in flow path length between injector and producer well.

Concludingly, some statistical analysis is carried using the breakthrough time data of Figure 3.4. This is shown in Table 3.4. The sample standard deviations are calculated using equation (3.20), while the means are the averages of the breakthrough times in each N/G interval. The non-cyclical mean in the 20-30 % N/G interval of 74,9 years is notably higher than the cyclical mean of 56,6 years. This corresponds with Figure 3.4, where the non-cyclical subsamples have generally equal or slower breakthrough times. It is also notable that both the cyclical and non-cyclical standard deviations in the 30-40 % N/G interval is much lower relative to the standard deviations in the other intervals. This also corresponds to the data in Figure 3.4, with less scatter in the 30-40 % N/G interval compared to the other intervals.

N/G interval	Cyclical mean (years)	Non-cyclical Mean (years)	Cyclical Stdev (years)	Non-cyclical Stdev (years)
10-20 %	44,1	48,3	12,9	13,3
20-30 %	56,6	74,9	11,5	13,6
30-40 %	81,5	76,0	8,6	9,6

Table 3.4: Statistical analysis from the data of Figure 3.4. The breakthrough time mean and standard deviations of each cyclical and non-cyclical N/G interval is determined. Notably the 20-30 % N/G interval non-cyclical mean is much higher. Both the cyclical and non-cyclical standard deviations in the 30-40 % N/G is much lower than the other intervals.

Temperature breakthrough curves

This shorter flow path hypothesis for the cyclical model is supported by the temperature breakthrough curves of Figure 3.6. This figure sets out a curve of the temperature in the production well vs simulation time, with on the left the non-cyclical breakthrough time curves and on the right the cyclical breakthrough time curves.

First of all it shows that the breakthrough time is mostly later for the non-cyclical model, since more curves are located in the top right of the left graph. The production temperature for the non-cyclical model drops much later with curves being mostly similar to the cyclical model. This could mean that the connectivity is similar, but the non-cyclical production wells just take longer to reach. More certainty about this could be created with longer curves, but it is capped by the run time. The run time can't be much longer since that causes a pressure overload in the simulation.
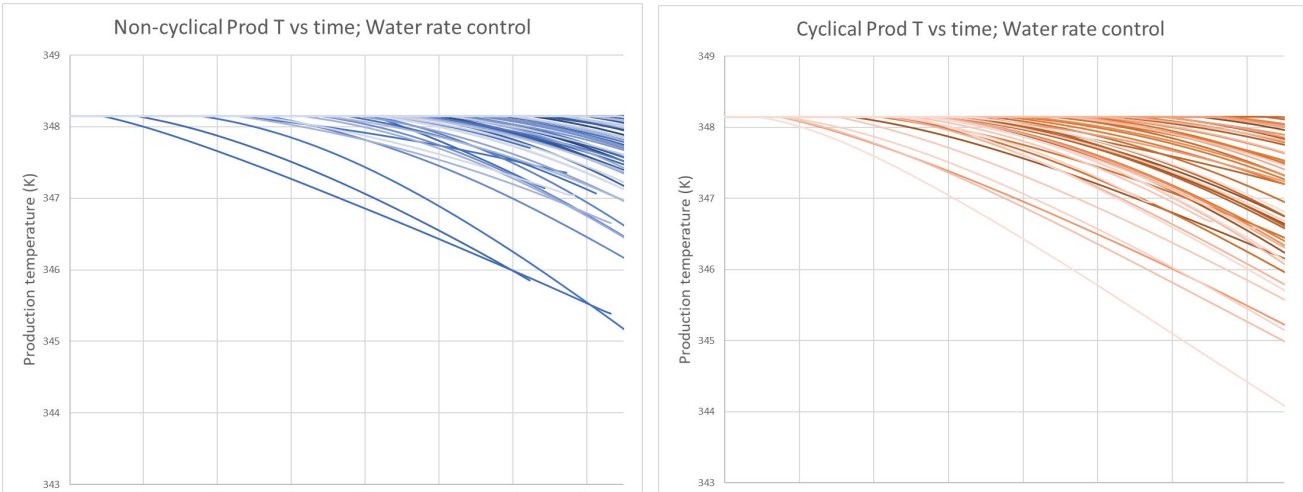
Figure 3.5: Temperature breakthrough curve using water rate as a control. Production temperature (K) is set out against simulation time (years). On the left the non-cyclical subsamples are set out, while on the right the cyclical subsamples are set out. More of the non-cyclical model breakthrough curves are situated on the top right, signaling more of the subsamples have slower breakthrough times.

Permeability differences

(Figure 3.6). A block of X = 5 km, Y = 6 km and Z = 60 m is chosen from the subsampling area discussed in Table 3.1 to compare the permeability differences in the cyclical and non-cyclical model. Figure 3.6 shows two representative permeability layer maps with the cyclical model on the left, and the non-cyclical model on the right. Both layer maps were chosen for having a similar amount of sand/N/G available.

In the figure the blue blocks portray clay with a permeability of 5mD while the other pink, red, orange and yellow blocks portray higher permeabilities sometimes reaching more than 3000 mD. The left layer graph shows the cyclical model which has much more clumped up sands relative to the right layer graph of the non-cyclical model. The non-cyclical model layer graph on the right side has much more clay between its sands. This supports the idea that overall there are less detours for reaching the production well in the cyclical model subsamples. Thus the permeability differences in the cyclical and non-cyclical models give support to the notion that the flow paths in the non-cyclical model are longer and need to take more detours
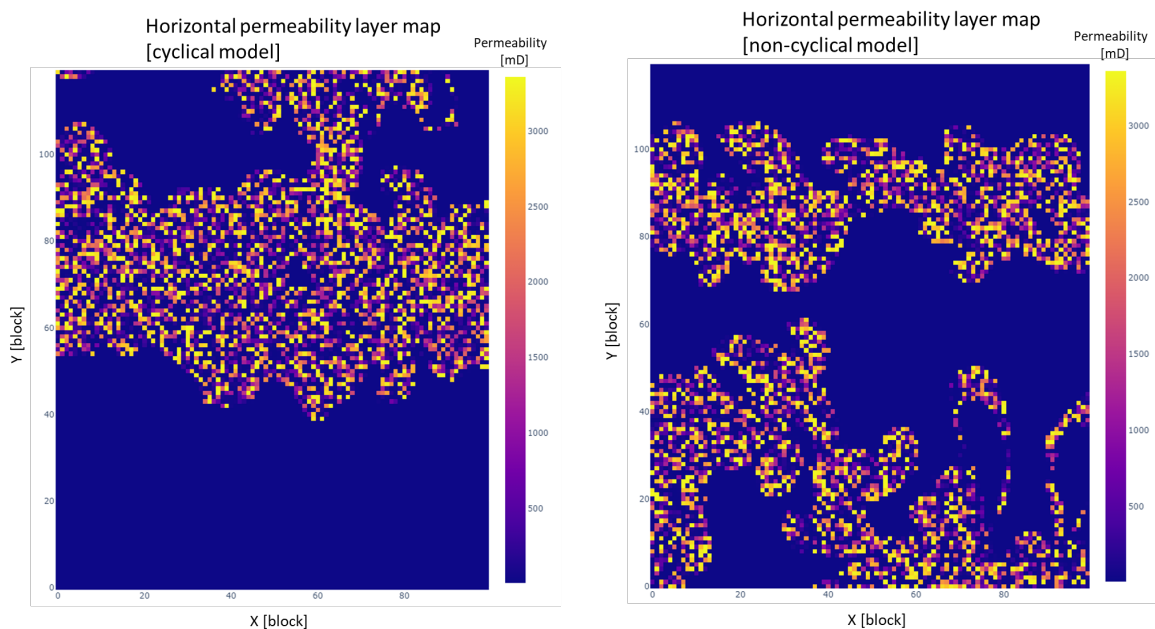
Figure 3.6: Representative horizontal permeability layer maps of the cyclical and non-cyclical subsampling areas discussed in Table 3.1. Both layer maps were chosen for having similar sand available. The blue portrays clay with a permeability of 5 mD, while the pink, red, orange and yellow portrays higher permeabilities sometimes reaching more than 3000 mD. It shows the difference in sand body vs clay distribution.

Temperature exchange between sand and clay bodies

Another hypothesis that could affect the breakthrough time is that there is a difference in temperature exchanges between the sands and clays. The edges of the sand bodies in the non-cyclical model have much more surface contact with the surrounding clay compared to the cyclical model (Figure 3.6). This hypothesis can be tested by comparing the generated enthalpy in the cyclical and non-cyclical subsamples.

Enthalpy is conveniently thought of as the heat content of a substance. Or in other words the amount of energy within a substance that is available for conversion to heat (Moeller, 2012).

To compare the enthalpy 2 subsamples with identical N/G were chosen. These were the cyclical and non-cyclical subsamples which both have a N/G of 22,8 %. Figure 3.7 shows two enthalpy layer maps right in the middle of both subsamples (at layer 30). This depicts that while the shape of the colder "clot" is different (this changes per layer), there is not much difference in the amount of higher vs lower enthalpy. So it can be assumed that the temperature exchange between sands and clays in the cyclical and non-cyclical models are not a big factor influencing breakthrough time.
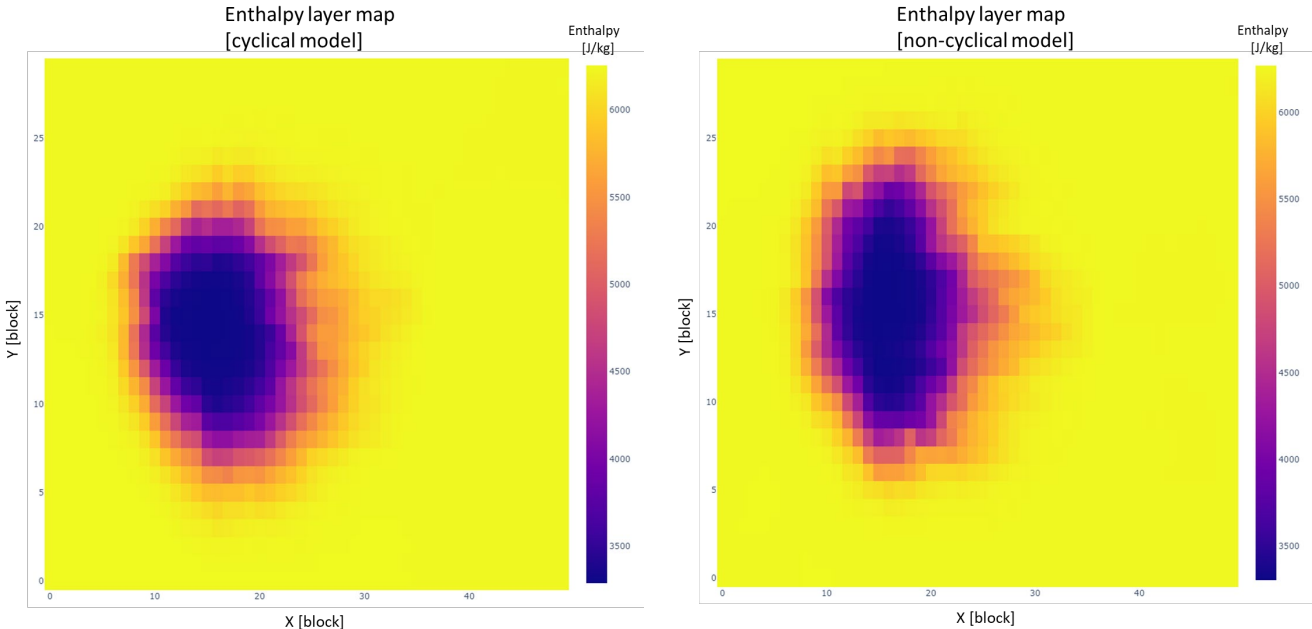
Figure 3.7: Enthalpy layer maps of a cyclical and a non-cyclial subsample with identical N/G (22,8 %). These layer maps are taken right in the middle of the subsample (at layer 30). It demonstrates that the amount of higher enthalpy vs lower enthalpy is not that different between the cyclical and non-cyclical model.

Outliers explained

There are some outliers in the subsamples visible in Figure 3.4 in which the N/G was set out against breakthrough time. These need some extra explanations. All these outliers come from non-cyclical subsamples. In Table 3.5 scenario 1 has a very low N/G compared to scenario 2, but they have a similar breakthrough time. Scenario 3 has the slowest, most economical breakthrough time. By looking at the geology or in this case permeability layer graphs these outliers can be explained.

Scenario	N/G (%) (sorted)	BHP difference (Bar) at 10,3k days simulation time step	Breakthrough time (years)
1	13,7	34,6	64
2	39,1	6,8	70
3	25,1	9,8	101

Table 3.5: Outliers from the subsamples visible in Figure 3.4. Scenario 1 has a very low N/G compared to scenario 2, but they have similar breakthrough times. Scenario 3 is the most economical subsample with the highest breakthrough time measured.

A higher BHP difference in scenario 1 relative to scenario 2 (Table 3.5) means there is less connectivity in scenario 1. This is because a higher BHP difference, while having the same fixed water flow rate, signifies there is less space connected between injector and producer well, causing a higher pressure

difference. Less connectivity should mean a slower breakthrough time in scenario 1 relative to scenario 2, but since there is way more sand in most of the connected layers in scenario 2 the two breakthrough times are still not far off. Way more sand in scenario 2 means the water has much more space to flow through before ending up in the producer well, causing the water the breakthrough time to be similar to scenario 1, while having more connectivity.

Scenario 3 is considered the most economical subsample since this subsample has the slowest breakthrough times of all subsamples. The N/G and BHP difference of this scenario is in between the first two scenarios. This means that scenario 3 should have a connectivity in between those of the other two scenarios. Looking at permeability layer graphs, the explanation for why scenario 3 still has the slowest breakthrough time is as follows (Figure 3.8). A lot of this subsample's layers, much more so than in the other 2 scenarios, have permeability layer graphs as depicted in Figure 3.8. This figure shows 2 examples of horizontal permeability layer maps of scenario 3 showing lots of detours for the flow path. This, combined with still having a reasonable amount of sand available (N/G: 25,1 %) is determined to be the main reason for the slow relative breakthrough time compared to the other subsamples.
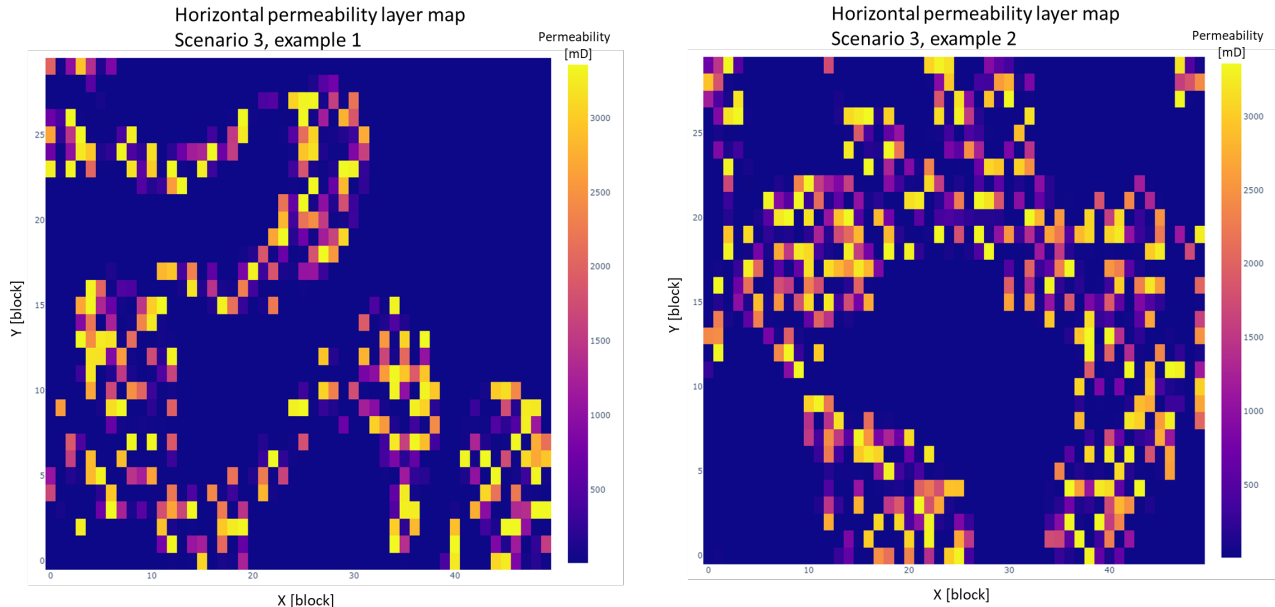
Figure 3.8: Two examples of horizontal permeability layer maps of scenario 3 (Table 3.5). The blue signifies clay, while the yellow, pink and purple is sand having variable permeability. It shows that there are lots of detours present in scenario 3, more so than in scenario 1 and 2.

3.3.2 BHP control simulation results

Besides using fixed water flow rate as a well control it is also possible to use fixed BHP or well pressure as a well control. Since the BHP well control results aren't as relevant to answering the aim of this thesis only the figure with N/G set out vs breakthrough time is explained. This answers most of the differences between using BHP vs water rate as a well control.

N/G set out vs breakthrough time

Figure 3.9 presents the N/G vs breakthrough time results for the hypothetical cyclical and hypothetical non-cyclical subsamples using a fixed BHP well control. The same subsamples were used as with the water rate control simulations. Contrary to the results in Figure 3.4 in which water rate was used as a well control, the correlations are inversed. A lower N/G shows to have a generally slower breakthrough time.

The reason for this is that using fixed BHP as a well control does not directly control the actual water rate flowing from injector to producer. A lower N/G means there is less sandy reservoir space available, causing the water rate to be lower to maintain a fixed BHP in the reservoir. This means water flows slower to the producer well, resulting in a generally slower breakthrough time. This is generally true for a lot of subsamples in Figure 3.9, but there are a lot of exceptions and the scatter is wide for both the cyclical and non-cyclical subsamples. Causes for these exceptions could be differences in the flow paths of these subsamples.
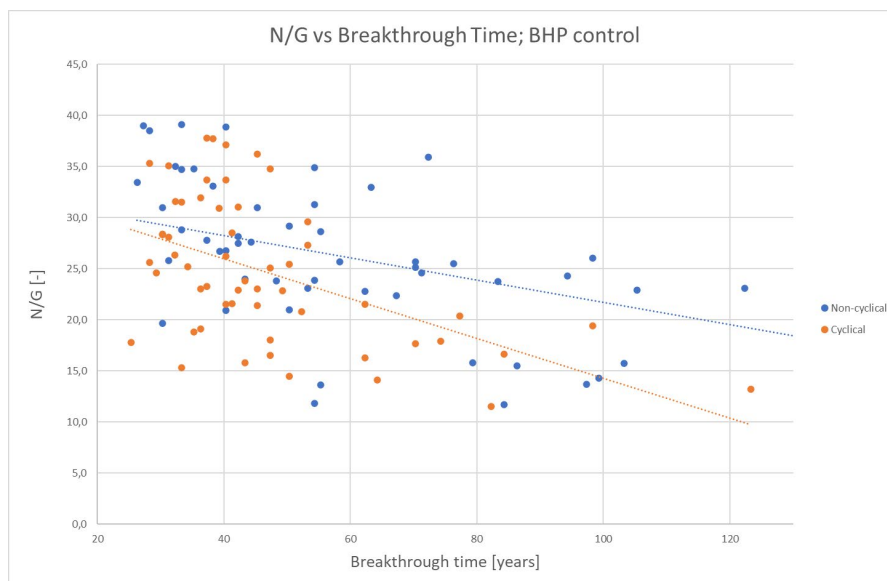
Figure 3.9 : Simulation results of the 21 cyclical and 21 non-cyclical subsamples. Using BHP as a well control N/G is plotted vs breakthrough time. Generally, a lower N/G gives a slower breakthrough time. This is not always the case, since the scatter is wide for both the cyclical and non-cyclical subsamples.

4.   Discussion

This research was set out to evaluate the impact of cyclical versus non-cyclical fluvial sedimentation on geothermal flow. In the first part of the thesis static facies modelling was done using Flumy to create generic hypothetical cyclic and hypothetical non-cyclical alluvial architecture models. It was found Flumy succeeded in that job through varying local and regional avulsion periods and it displayed the differences well. As such it served well for the scope of this study. The cyclical and non-cyclical models are hypothetical, since they are different from those created in previous work by Abels et al, 2013 and Wang et al, 2021. Limitations in the static models were present which are discussed in subsection 4.3. It was found that when comparing cyclical and non-cyclical models with similar N/G the main difference is in the shape of the sandstone body depositions. The cyclical model has overall thicker, laterally wider sand bodies. The non-cyclical model has thinner, less wide, but more often connecting sand bodies. Looking at the impact of the different sandstone body stratigraphies of the cyclical and non-cyclical models on geothermal flow the results are as follows. It was discovered that the main factor distinguishing the cyclical and non-cyclical models was overall equal or shorter cyclical model flow paths between the injector and producer well in a geothermal doublet. This was mainly true for the studied subsamples with a N/G of between 20 and 30 %. These findings are discussed in more detail below.

4.1 Cyclical vs non-cyclical static models

Evaluating the constructed hypothetical non-cyclical models, there are several differences between the different runs. The runs are differentiated by varying local avulsion periods. This causes the runs with lower local avulsion periods to have a larger N/G, since more avulsion occurs (Table 2.7). More avulsion causes more incision into the floodplain and thus a larger N/G. As expected, the runs where avulsion occurs more often also cause less isolated sand bodies and fewer vertically thinner sand bodies. This is clearly depicted in the cross-section in Figure 2.7. This is in contrast to the cross section in Figure 2.11, where much less avulsion occurred, which causes thicker, more isolated sand bodies. The difference in vertical sand body thickness is not huge though, as depicted in Table 2.7. The maximum thickness difference between all the runs was only 5 meters.

Besides the difference in the regional and local avulsion parameter, the non-cyclical model has one other different parameter value. The maximum sediment thickness, which controls the thickness of the floodplain deposits, is uniform between 0.2 and 0.6 m. In contrast, the cyclical model has a constant value of 0.2 m. This had to be done, otherwise the non-cyclical would have far too much sand deposited compared to the cyclical model. This is shown in Figure 2.12 and 2.13.

There is some variability, especially in the non-cyclical model. To test this, 5 extra identical runs of original non-cyclical Run 5 (Figure 2.8) were conducted. It was determined that the additional runs were not that different from the original run. The cross sections were similar with all of them having accumulating sand bodies, and with a largest N/G difference of 2.5 % (Table 2.8).

It should also be mentioned that there was a fairly big difference in run time vs the amount of sediment deposited in the non-cyclical runs. Non-cyclical Runs 1, 2 and 3 with local avulsion periods of 500, 1000 and 1500 (Table 2.7) had similar run times vs the amount of deposition relative to the cyclical runs. Non-cyclical Runs 4 to 8 with longer avulsion periods had shorter run times with Run 8 being about two-thirds shorter. When less avulsion occurs, more flooding happens and that shortens the run time.

The two hypothetical cyclical model run results only differ in resolution and the way Flumy makes different realizations through stochastics. Following the hypothesis that orbital forcing causes cyclic deposition to be in specific precession cycles of about 20000 years (Abels et al, 2013) there was no need to test out changes in the regional avulsion parameter. As expected, the cyclical runs are similar since they are different realizations while having the same input parameters, only Cyclical Model 2 has a lower horizontal resolution. They have similar Net to Gross, only differing 1.7%. The sand bodies also have similar vertical thicknesses, only differing about 2 meters (Table 2.9). The difference lies in which positions/locations the sand bodies are deposited inside the domain. Looking at cross-sections of Figure 2.21 vs Figure 2.22, Cyclical Model 1 has more deposition closer to the edges. This is argued to be because the starting position of the first sand body deposition was also closer to the edge of the domain. This causes a difference in connectivity, in which Cyclical Model 2 seems to have relatively less connectivity between the sand bodies (Figure 2.22). This difference could be debated since the N/G of both runs are about 28%, which might be big enough such that the sand bodies are still connected anyway.

A big difference when comparing the cyclical model results in this thesis to similar studies of cyclical modelling (Abels et al, 2013) (Wang et al, 2021) is that there is no defining difference between an overbank and avulsion phase present. These phases are portrayed in Figure 1.2 (Abels et al, 2013).

Discussing the difference between the hypothetical cyclical and hypothetical non-cyclical runs, it is best to compare those with similar properties. Non-cyclical Run 5 (Figure 2.8) is chosen to compare to the cyclical model run 2 (Figure 2.22) since it has similar Net to Gross of 28,4% vs 27,4%/29,7% (Table 2.7 and Table 2.9). It also has a similar vertical sand body thickness, where non-cyclical Run 5 only has about 3 meters less thick sand bodies averagely versus the cyclical models. Both of these cyclical and non-cyclical model runs are also chosen for geothermal flow modelling and from now on are addressed as the chosen cyclical and non-cyclical models. The chosen non-cyclical model has a fairly long local avulsion period of 3000 years. Looking at Figure 2.8 and 2.22, both types of models have a similar average sand body vertical thickness. The main difference lies in the shape of the sand bodies. The cyclical model has overall thicker, laterally wider sand bodies. The non-cyclical model has thinner, less wide, but more often connecting sand bodies. Counting accumulated sand bodies, overall the cyclical and non-cyclical model have similar sand body thicknesses. Lastly, a difference in connectivity could not be adequately determined between the static chosen cyclical and non-cyclical models.

4.2 Impact of the cyclical and non-cyclical models on geothermal flow

Geothermal flow modelling using DARTS was done on subsamples of the cyclical and non-cyclical models. The subsampling methodology is explained in Table 3.1. There are two well controls possible to use in DARTS, water rate and BHP. Using water flow rate as a well control gives more realistic results since this is also how wells are controlled in real world geothermal doublets. Only the results using a fixed water rate well control are discussed in this chapter.

Setting out the N/G against the BHP well difference at a fixed certain point in time of all the subsamples gives the trend that a lower N/G means that the measured BHP becomes higher and vice versa (Figure 3.3). This trend is especially visible in subsamples with a N/G of between 20 and 40 %. The trend is logical since a lower N/G means less reservoir space, and with fixed water flow rate it causes higher pressures. In the N/G range of between 20 and 40 %, the is similar, with little scatter and outliers. The hypothesis is then that the connectivity of the subsamples in that range must also be similar, when comparing subsamples with similar N/G. Regarding subsamples with a N/G of between 10 and 20 %, the scatter becomes high and it seems the BHP difference is high or low, irrespective of the N/G of the subsample. This result follows the hypothesis that between 10-20 % N/G the connectivity is most sensitive (more prone to change) in fluvial systems (Crooijmans et al, 2016). It also gives credit to the

hypothesis that since allogenic and autogenic behaviour is ordered, there is a comparable amount of connectivity in both.

When setting out the N/G against the breakthrough time of all the subsamples, it gives the trend that generally a lower N/G means a faster breakthrough time for both the cyclical and non-cyclical subsamples (Figure 3.4). This trend is expected, since a lower N/G means there is less reservoir space for the water to flow to before reaching the producer well and vice versa. There is a lot of scatter present all over the graph with many outliers. It is also visible that different N/G intervals give different breakthrough results, when comparing the cyclical and non-cyclical models. Especially in the N/G interval between 20 and 30 %, the non-cyclical subsamples have a generally equal or slower breakthrough time compared to the cyclical subsamples.

Since it does not seem likely that connectivity is the deciding factor in the generally equal or slower non-cyclical (compared to cyclical) breakthrough times in the 20-30 % N/G range, it creates the hypothesis that there is a difference in flow path length between injector and producer well. Specifically the flow paths in the cyclical model are equal or shorter. This hypothesis is supported by the temperature breakthrough curves in Figure 3.5. This shows that the cyclical and non-cyclical curves are similar but most non-cyclical subsamples just take longer to get similar curves. This means that the connectivity is similar, but the non-cyclical subsamples take longer to reach. Permeability layer graphs of the cyclical and non-cyclical models (Figure 3.6) also point toward the difference in flow path hypothesis. Figure 3.6 shows horizontal permeability layer graphs of the areas from which both cyclical and non-cyclical subsamples are taken. This shows that generally the cyclical model has much more accumulated sandstone bodies compared to the non-cyclical model. This means that generally the flow path is much more direct in the cyclical subsamples compared to the non-cyclical subsamples in which more detours need to be taken. This is also in line with the hypothesis that autogenic and allogenic controls affect sand body and shale thicknesses. And that these are factors that influence the lifetime and doublet performance of a geothermal reservoir (Crooijmans et al, 2016). Producing 3D streamlines which visualize the flow paths which would help a lot to credit the difference in flow paths hypothesis, but this would cost a lot more time and is a recommendation for the future. A study on 2D streamlines in geothermal flow was carried out by Tahir, A, 2019, but not yet on 3D streamlines.

Another reason for the different breakthrough times in Figure 3.4 could be that there is a difference in temperature exchange between the sands and clays in the cyclical and non-cyclical model. The hypothesis would be that since the cyclical sands are more accumulated, they have less surface contact area with the clays compared to the non-cyclical model. This would mean that since there is more temperature exchange in the non-cyclical model, causing slower breakthrough times. This hypothesis is assumed to be false since the enthalpy in both cyclical and non-cyclical subsamples seem to be similar (Figure 3.7).

Lastly, the case of the most economical subsample with the slowest breakthrough time is studied . This non-cyclical subsample has an average N/G (25,1 %) and a breakthrough time of 101 years (Table 3.5). The expectation would be that the most economical subsample would have one of the highest measured N/G, but this is not the case. The main reason for why this subsample is still the most economical seems to be that this specific subsample has a lot of sands bodies which cause long detours in the well connections (Figure 3.8). This causes a longer flow path length leading to slower breakthrough times. Whether this specific situation can also be also found in the real world remains to be seen. In theory this is possible since there is no odd boundary effect present which could affect the geothermal flow.

4.3 Limitations

There are methods that could be done, which might generate more realistic alluvial architecture models in Flumy. One of these options is well conditioning. Using core analysis wells could be inputted into Flumy to create closer to reality deposition. Using well conditioning e.g. a point bar must be deposited at a well location at a specific time. This would in theory create environments similar to a specific place if that place has a lot of well data present in that location. Still, this does not seem to be trustworthy option, since that essentially forces certain conditions on the layers around conditioned well data. This is also not possible for the purpose of this thesis since more general cyclical and non-cyclical models are created with no well data.

Another improvement that could be made to create models more closer to reality is to vary certain parameters over time. This would create the effect that parameters such as channel dimensions or avulsion periods can change over time, which is closer to how it is in reality. This can be done by pausing the simulation, and changing the necessary parameters. The channel dimensions are fixed without this method. This might also help to model more distinct overbank phases and avulsion phases visible in previous models made on cyclical successions (Abels et al, 2013) (Wang et al, 2021). This method is not performed in this thesis since that would complicate it a lot and it would take a lot more time. This is a recommendation for further studies using Flumy.

A different limitation using Flumy is that it does not create a natural, physics based river which process-based models do. Software such as Delft3D does this and could be a recommendation for the future.

Lastly, there are some limitations using DARTS to carry out the thesis objective. First of all the total cyclical and non-cyclical models were too large to model with DARTS. Only small parts could be loaded in otherwise the processing power was not enough. This is why both cyclical and non-cyclical models were subsampled. The subsampling needs to be representative, otherwise no proper comparison between models can be made. Ultimately, it would be better to get more subsample data.

When using water rate as opposed to BHP as a well control, the outcome is more accurate to how it is in reality, since it is also how real world geothermal doublets are controlled. A limitation is then that water rate control simulations often have a narrow window in which a breakthrough time could be produced, without pressure inflating too much in the model. This is opposed to the BHP well control simulations, where this window is much bigger.

5. Conclusions & recommendations

Evaluation reveals that the impact of cyclical versus non-cyclical fluvial sedimentation on geothermal flow is significant. In the first part of the study a hypothetical cyclical and hypothetical non-cyclical model were created and chosen for comparison. This was done using process-imitating and stochastic modelling software Flumy. It was determined that Flumy was suitable to produce the models for the scope of this study through varying local and regional avulsion periods and it displays the differences well. The cyclical and non-cyclical models are hypothetical, since they are different from cyclical succession models in previous work by Abels et al, 2013 and Wang et al, 2021. When comparing the static cyclical and non-cyclical models with similar N/G it was determined that the main difference is in the shapes of the sandstone body stratigraphy. The cyclical model has overall thicker, laterally wider sand bodies. The non-cyclical model has thinner, less wide, but more often connecting sand bodies. Counting accumulated sand bodies, overall the cyclical and non-cyclical model have similar sand body thicknesses.

Evaluating the impact on geothermal flow shows a few factors distinguishing the cyclical and non-cyclical models. When considering similar N/G, cyclical and non-cyclical model subsamples in the 20-40 % N/G range give similar BHP/well pressure at the same fixed water rate. This points to the hypothesis that, at comparable N/G, the connectivity between producer and injector well must then also be similar. Regarding breakthrough times of the model subsamples, in the N/G range of between 20-30 % N/G the non-cyclical subsamples have a generally equal or slower breakthrough time compared to the cyclical subsamples. This gives credit to another hypothesis, which is that the cyclical model must than have overall equal or shorter flow paths between the well connections in the geothermal doublet.

Definitely proving the difference in flow path hypothesis can best be done using 3D streamlines. Streamlines can visualize the flow paths leading from the injector to producer well and can visualize areas of higher and lower water flow rate. Visualizing 3D streamlines is complicated and time consuming and is a recommendation for the future. Another recommendation is to collect more subsample data to give more credence to the flow path difference hypothesis.

An improvement to the created static models by Flumy is to vary parameters such as the channel dimensions and avulsion periods over time. This would help to model more distinct overbank phases and avulsion phases visible in previous models done on cyclical successions. This wasn't done due to time constraints and it would complicate it a lot.

Lastly, instead of using Flumy models more complicated process-based models could be realized. Process-based fluvial modelling using e.g. Delft3D simulates a natural, physics based river which would be more accurate to real word rivers.

Bibliography

Abels, H. A., Kraus, M. J., & Gingerich, P. D. (2013). Precession-scale cyclicity in the fluvial lower Eocene Willwood Formation of the Bighorn Basin, Wyoming (USA). *Sedimentology*, *60*(6), 1467-1483.

Gouw, M. J. P. (2007). Alluvial architecture of fluvio-deltaic successions: a review with special reference to Holocene settings. *Netherlands Journal of Geosciences/Geologie en Mijnbouw*, *86*(3).

Karssenberg, D., & Bridge, J. S. (2008). A three-dimensional numerical model of sediment transport, erosion and deposition within a network of channel belts, floodplain and hill slope: extrinsic and intrinsic controls on floodplain dynamics and alluvial architecture. *Sedimentology*, *55*(6), 1717-1745.

Hajek, E. A., Heller, P. L., & Schur, E. L. (2012). Field test of autogenic control on alluvial stratigraphy (Ferris Formation, Upper Cretaceous–Paleogene, Wyoming). *Bulletin*, *124*(11-12), 1898-1912.

Stouthamer, E. and Berendsen, H.J.A.(2007) Avulsion: the relative roles of autogenic and allogenic processes. *Sed. Geol.*, 198, 309–325.

Villamizar, C. A., Hampson, G. J., Flood, Y. S., & Fitch, P. J. (2015). Object-based modelling of avulsion-generated sandbody distributions and connectivity in a fluvial reservoir analogue of low to moderate net-to-gross ratio.

Bubnova, A (2018). On the conditioning of process-based channelized meandering reservoir models on well data. Ph. D. Thesis PSL University, 181 p.

Grant, M. (2013). *Geothermal reservoir engineering*. Elsevier.

Willems, C. J., Nick, H. M., Donselaar, M. E., Weltje, G. J., & Bruhn, D. F. (2017). On the connectivity anisotropy in fluvial Hot Sedimentary Aquifers and its influence on geothermal doublet performance. Geothermics, 65, 222-233.

Kane, I. A., McCaffrey, W. D., & Martinsen, O. J. (2009). Allogenic vs. autogenic controls on megaflute formation. *Journal of Sedimentary Research*, *79*(9), 643-651.

Miall, A. D. (2014). *Fluvial depositional systems* (Vol. 14). Berlin: Springer.

Willems, C. J., Vondrak, A., Munsterman, D. K., Donselaar, M. E., & Mijnlieff, H. F. (2017). Regional geothermal aquifer architecture of the fluvial Lower Cretaceous Nieuwerkerk Formation–a palynological analysis. *Netherlands Journal of Geosciences*, *96*(4), 319-330.

WILLEMS, Cees. *Doublet deployment strategies for geothermal Hot Sedimentary Aquifer exploitation.* s.l. : Ph.D Thesis, 2017.

Willems, C. J., Nick, H. M., Donselaar, M. E., Weltje, G. J., & Bruhn, D. F. (2017). On the connectivity anisotropy in fluvial Hot Sedimentary Aquifers and its influence on geothermal doublet performance. *Geothermics*, *65*, 222-233.

Foreman, B. Z., Heller, P. L., & Clementz, M. T. (2012). Fluvial response to abrupt global warming at the Palaeocene/Eocene boundary. *Nature*, *491*(7422), 92.

Lopez, S., Galli, A., & Cojan, I. (2001, September). Fluvial meandering channelized reservoirs: a stochastic and process based approach. In *2001 Annual conference of the IAMG, Cancun (Mexico), Sept* (pp. 6-12).

Lopez, S., Cojan, I., Rivoirard, J., Galli, A., 2008. Process-Based Stochastic Modelling: Meandering Channelized Reservoirs, in: Analogue and Numerical Modelling of Sedimentary Systems: From Understanding to Prediction. Wiley-Blackwell, pp. 139–144. https://doi.org/10.1002/9781444303131.ch5

Wang, Y., Khait, M., Voskov, D., Saeid, S., & Bruhn, D. (2019). Benchmark test and sensitivity analysis for Geothermal Applications in the Netherlands. In *44th Workshop on Geothermal Reservoir Engineering, Stanford, California. Qatar National Research Fund• Yang Wang• Stephan de Hoop*.

DARTS (2019): Delft Advanced Research Terra Simulator. In *https://darts-web.github.io/darts-web/*

Voskov, D. V. (2017). Operator-based linearization approach for modeling of multiphase multi-component flow in porous media. *Journal of Computational Physics*, *337*, 275-288.

Khait, M., & Voskov, D. (2018a). Operator-based linearization for efficient modeling of geothermal processes. *Geothermics*, *74*, 7-18.

Khait, M., & Voskov, D. (2018b). Adaptive parameterization for solving of thermal/compositional nonlinear flow and transport with buoyancy. *SPE Journal*, *23*(02), 522-534.

Wong, Z. Y., Horne, R., & Voskov, D. (2015). *A geothermal reservoir simulator in AD-GPRS* (Doctoral dissertation, Stanford University).

Faust, C. R., & Mercer, J. W. (1975). Summary of Our Research in Geothermal Reservoir Simulation. In *Proc. Workshop on Geothermal Reservoir Engineering, Stanford University, Stanford, CA, SGP-TR-12*.

Crooijmans, R. A., Willems, C. J. L., Nick, H. M., & Bruhn, D. F. (2016). The influence of facies heterogeneity on the doublet performance in low-enthalpy geothermal sedimentary reservoirs. *Geothermics*, *64*, 209-219.

Hamm, V., & Lopez, S. (2012, January). Impact of fluvial sedimentary heterogeneities on heat transfer at a geothermal doublet scale. In *Stanford Geothermal Workshop* (pp. SGP-TR).

Gries, S. (2015). *System-AMG approaches for industrial fully and adaptive implicit oil reservoir simulations* (Doctoral dissertation, Universität zu Köln).

Shetty, S., Voskov, D., & Bruhn, D. (2017). *Numerical Strategy for Uncertainty Quantification in Low Enthalpy Geothermal Projects* (Doctoral dissertation, M. Sc. thesis. Department of Applied Earth Science. Delft University of Technology).

Okandan, E. (Ed.). (2012). *Geothermal reservoir engineering* (Vol. 150). Springer Science & Business Media.

Wang, Y., Khait, M., Voskov, D., Saeid, S., & Bruhn, D. (2019). Benchmark test and sensitivity analysis for geothermal applications in the netherlands. In *Workshop on Geothermal Reservoir Engineering.*

Moeller, T. (2012). *Chemistry: with inorganic qualitative analysis*. Elsevier.

Wachowicz-Pyzik, A., Sowiżdżał, A., Pająk, L., Ziółkowski, P., & Badur, J. (2020). Assessment of the Effective Variants Leading to Higher Efficiency for the Geothermal Doublet, Using Numerical Analysis–Case Study from Poland (Szczecin Trough). *Energies*, *13*(9), 2174.

Wang, Y., Storms, J. E., Martinius, A. W., Karssenberg, D., & Abels, H. A. (2021). Evaluating alluvial stratigraphic response to cyclic and non-cyclic upstream forcing through process-based alluvial architecture modelling. *Basin Research*, *33*(1), 48-65.

Tahir, A. (2019). *Proxy-model for Flow and Transport in Geothermal Reservoirs.* MSc thesis.

Duncan, K. W. (1979). Obtaining the overall mean and variance for combined samples.

Appendix

Cross sections of cyclical model 1 in the X,Y-plane.

Figure A.1 Panel A

Z = 1 m | Z = 10 m | Z = 20 m
Z = 30 m | Z = 40 m | Z = 50 m
Z = 60 m | Z = 700 m | Z = 800 m
Z = 90 m | Z = 100 m

A

30 km
100 m
15 km
X
y
Z

B
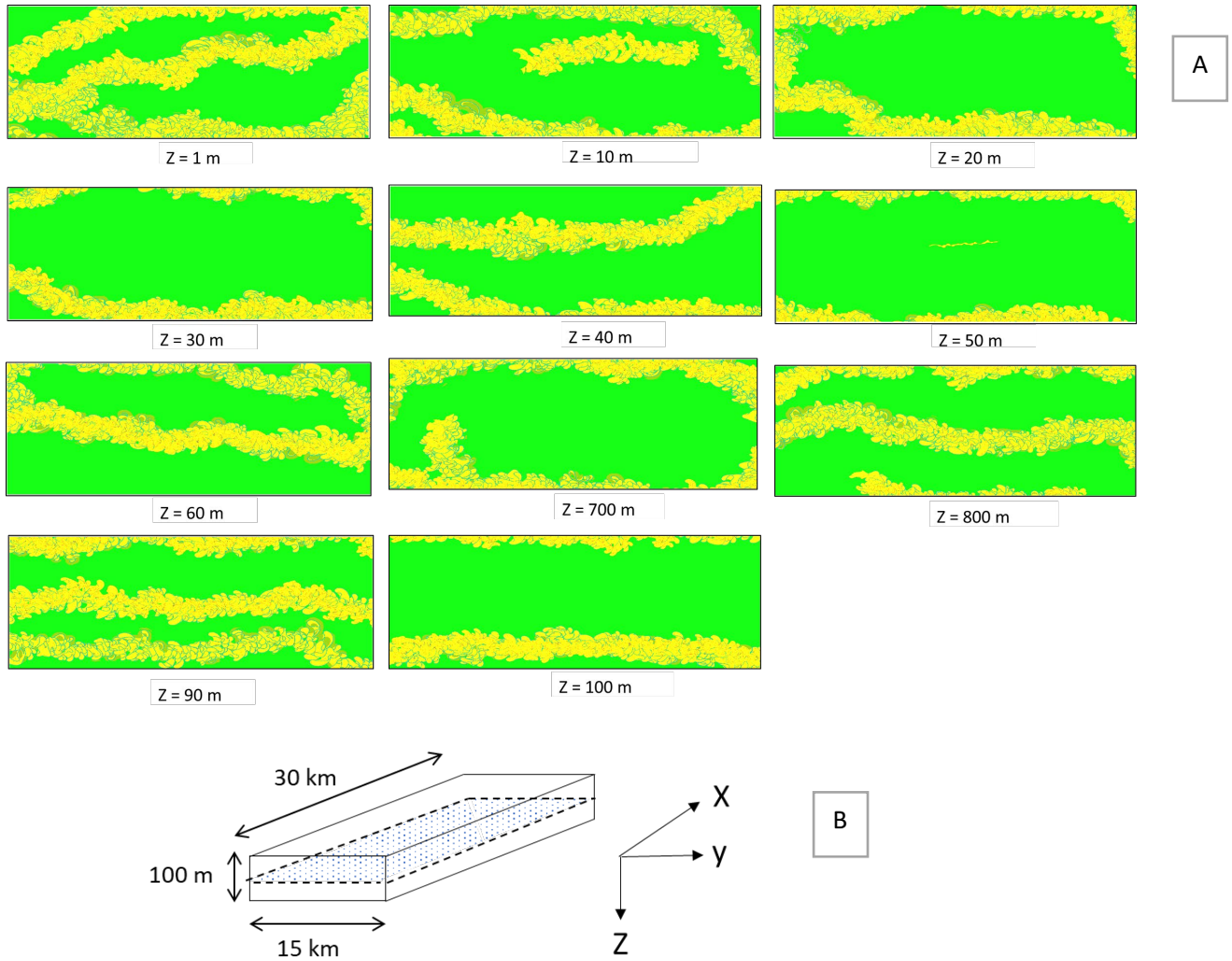
Figure A.1: Cyclic model 1. Panel A show multiple facies cross sections in the X,Y-plane (from the top) of Cyclic model 1. This is clarified in panel B. Z = 1m means it is near the top of the 3D block, and Z = 100m means it is near the bottom. It can be noticed how the connectivity changes when moving through the cross-sections. There does not seem to be much correlation between the cross sections, other that sometimes the sand bodies connect, and sometimes they don't.

Geothermal modelling results in table form

Water rate control; Cyclical model			Water rate control; Non-cyclical model		
N/G (sorted)	BHP diff (-)	BT (years)	N/G (sorted)	BHP diff (-)	BT (years)
11,5	21,2	47	11,7	22,5	45
13,2	33,1	46	11,8	21,0	29
13,9	48,5	43	11,9	50,3	62
14,1	19,0	35	13,6	22,8	25
14,5	19,5	28	13,7	34,6	64
15,3	15,3	28	13,7	19,5	61
16,3	18,0	42	13,8	45,1	61
16,5	13,4	53	14,3	21,7	58
16,7	20,0	51	15,5	24,4	43
17,7	16,6	53	15,8	31,2	43
17,8	12,6	25	15,8	20,5	47
17,9	18,3	45	19,7	10,4	38
18,0	15,4	37	20,9	10,5	54
18,8	12,0	41	21,0	10,1	70
19,1	10,4	48	22,4	12,7	73
19,4	16,7	79	22,8	11,8	76
20,4	29,2	28	22,9	15,2	90
20,8	14,9	48	23,1	16,9	100
21,4	11,5	54	23,1	11,2	65
21,5	11,2	48	23,8	12,4	86
21,5	14,6	54	23,8	12,2	59
21,6	11,3	49	23,9	10,7	68
22,8	10,6	64	24,0	10,0	62
22,9	10,6	56	24,3	12,7	95
23,0	10,6	48	24,6	13,4	77
23,0	13,3	42	25,1	9,8	101
23,3	10,7	50	25,5	11,9	87
23,8	10,5	58	25,7	10,7	83
24,6	8,8	48	25,7	14,6	71
25,1	9,3	68	25,8	7,9	54
25,2	8,2	66	26,0	15,7	90
25,5	11,2	65	26,7	9,1	67
25,6	8,2	50	26,8	8,5	67
26,2	9,8	64	27,5	8,6	67
26,3	9,5	50	27,6	8,3	75
27,3	11,2	66	27,8	8,6	61
28,1	8,4	60	28,1	7,6	79
28,3	7,6	61	28,6	9,3	80
28,4	8,7	52	28,8	8,8	52
28,5	9,1	73	29,2	8,7	80
29,6	9,6	85	31,0	7,7	82

30,9	7,6	79	31,0	6,9	63
31,0	7,0	93	31,3	9,2	90
31,5	7,4	74	33,0	11,1	79
31,6	6,9	71	33,1	6,9	85
32,0	7,6	69	33,4	6,3	66
33,7	7,0	79	34,7	6,4	71
33,7	6,9	87	34,8	7,2	72
34,8	7,6	95	34,9	8,2	87
35,1	6,6	75	35,0	6,1	73
35,3	6,3	70	35,9	10,4	64
36,2	8,0	84	38,5	5,6	76
37,1	7,0	88	38,9	6,8	92
37,7	6,4	87	39,0	6,0	66
37,8	6,4	86	39,1	6,8	70

Table A.1: The simulation results for the 55 cyclical and 55 non-cyclical subsamples are presented. The simulations are done using a fixed water rate as a well control. The N/G of both the cyclical and non-cyclical subsamples are sorted from low to high. This way it is possible to easier compare them against the breakthrough time and BHP at the producer well at a specific time step in the simulation. This time step is at 10,3k days. It is taken at the same time step for all the subsamples such that it is possible to compare them.

BHP control; Cyclical model			BHP control; Non-cyclical model		
N/G (sorted)	WR diff (m3/h)	BT (years)	N/G (sorted)	WR diff (m3/h)	BT (years)
11,5	3,7	82	11,7	3,6	84
13,2	2,4	123	11,8	3,8	54
14,1	4,0	64	11,9	1,7	220
14,5	3,9	50	13,6	3,5	55
15,3	5,0	33	13,7	2,3	152
15,8	5,6	43	13,7	4,0	97
16,3	4,3	62	13,8	1,8	245
16,5	5,7	47	14,3	3,6	99
16,7	3,9	84	15,5	3,2	86
17,7	4,6	70	15,8	2,6	103
17,8	6,0	25	15,8	3,8	79
17,9	4,1	74	19,7	7,2	30
18,0	4,9	47	20,9	7,1	40
18,8	6,4	35	21,0	7,4	50
19,1	7,1	36	22,4	6,0	67
19,4	4,6	98	22,8	6,4	62
20,4	2,6	77	22,9	5,0	105
20,8	5,1	52	23,1	4,6	122
21,4	6,6	45	23,1	6,7	53
21,5	6,6	40	23,8	6,0	83
21,5	5,2	62	23,8	6,2	48
21,6	6,6	41	23,9	6,9	54
22,8	6,9	49	24,0	7,3	43

22,9	7,0	42	24,3	5,8	94
23,0	6,9	36	24,6	5,6	71
23,0	5,6	45	25,1	7,7	70
23,3	10,7	37	25,5	6,4	76
23,8	7,1	43	25,7	7,0	58
24,6	8,3	29	25,7	5,3	70
25,1	7,8	47	25,8	9,1	31
25,2	8,8	34	26,0	4,8	98
25,5	6,7	50	26,7	8,0	39
25,6	8,8	28	26,8	8,6	40
26,2	7,5	40	27,5	8,5	42
26,3	7,8	32	27,6	8,6	44
27,3	6,7	53	27,8	8,4	37
28,1	8,7	31	28,1	9,6	42
28,3	9,5	30	28,6	7,9	55
28,4	8,3	30	28,8	8,2	33
28,5	8,2	41	29,2	8,3	50
29,6	7,6	53	31,0	9,3	45
30,9	9,4	39	31,0	10,3	30
31,0	10,2	42	31,3	7,9	54
31,5	9,7	33	33,0	6,6	63
31,6	10,3	32	33,1	10,4	38
32,0	9,4	36	33,4	11,2	26
33,7	10,1	37	34,7	11,0	33
33,7	10,4	40	34,8	9,8	35
34,8	9,4	47	34,9	8,5	54
35,1	10,7	31	35	11,4	32
35,3	11,1	28	35,9	6,8	72
36,2	9,0	45	38,5	12,4	28
37,1	10,0	40	38,9	10,5	40
37,7	10,9	38	39,0	11,6	27
37,8	10,8	37	39,1	10,3	33

Table A.2: The simulation results for the 55 cyclical and 55 non-cyclical subsamples are presented. The simulations are done using a fixed BHP as a well control. The N/G of both the cyclical and non-cyclical subsamples are sorted from low to high. This way it is possible to easier compare them against the breakthrough time and water rate at the producer well at a specific time step in the simulation. This time step is at 10,3k days. It is taken at the same time step for all the subsamples such that it is possible to compare them.

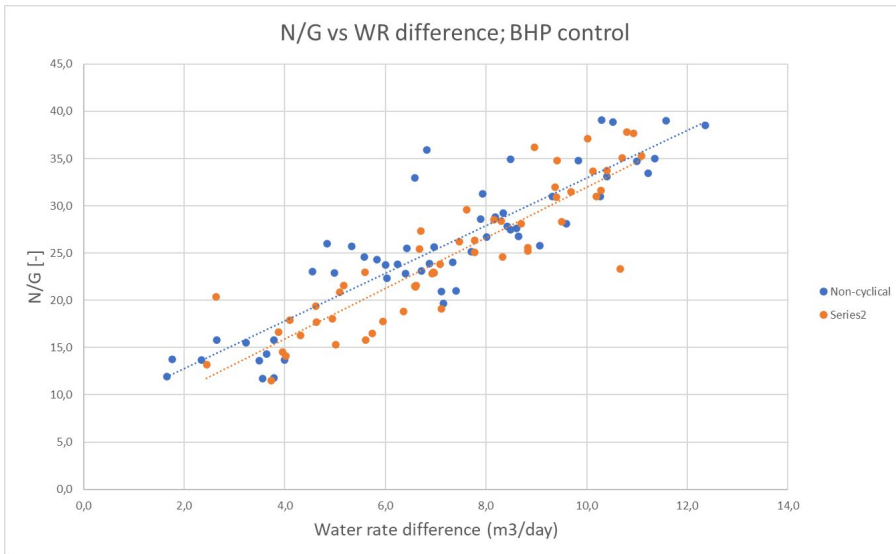**BHP well control extra geothermal results**

Figure A.2: N/G set out against the water rate well difference. The blue dots are non-cyclical subsamples, while the orange dots are cyclical subsamples. Using BHP as a well control N/G is plotted vs water rate at the producer well at a specific fixed time step in the simulation. This time step is taken at 10,3k days.
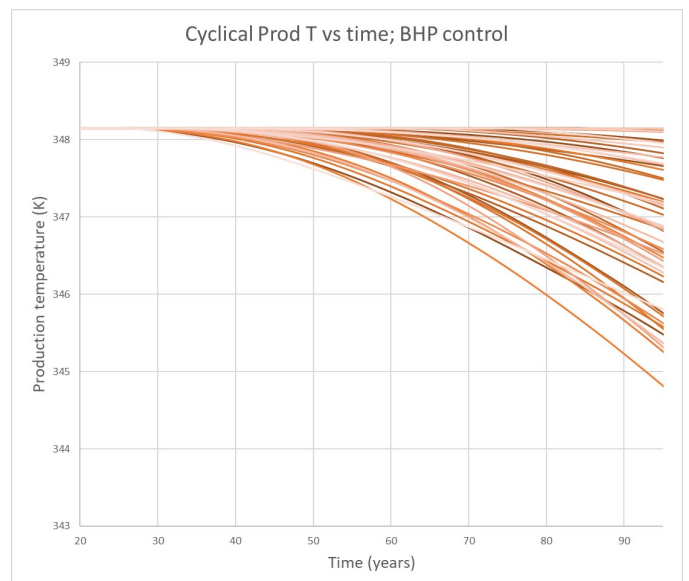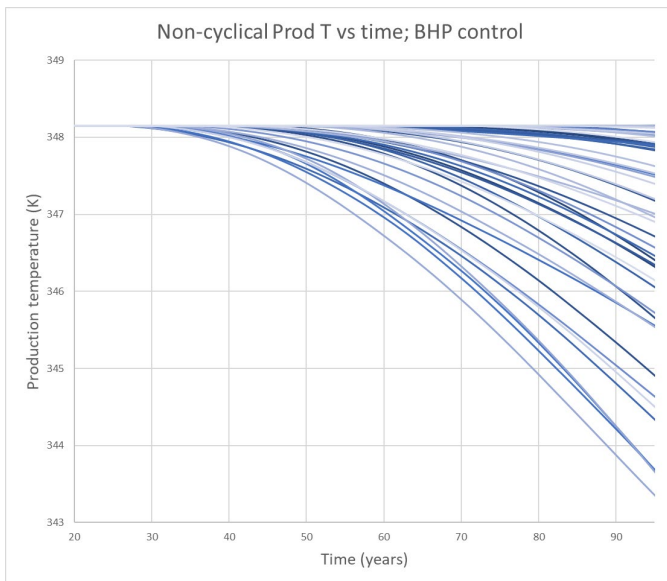

Figure A.3: Temperature breakthrough curve using BHP as a control. Production temperature (K) is set out against simulation time (years). On the left the non-cyclical subsamples are set out, while on the right the cyclical subsamples are set out.